Human parainfluenza virus infection remodels the host cell glycome

Plabon Kumar Das[1], Larissa Dirr[1], Benjamin Bailly[1], Patrice Guillon[1], Arun Everest-Dass[1] and Mark von Itzstein[1]

[1]Institute for Biomedicine and Glycomics, Griffith University, Gold Coast Campus, Queensland 4222, Australia.

Abstract

Human parainfluenza virus type 3 (HPIV-3) remains a major cause of respiratory illness particularly among young children, the elderly and immunocompromised individuals. Despite significant efforts in therapeutic discovery research, there is neither an effective antiviral nor a vaccine available against HPIV-3. Host cell glycosylation is known to play a pivotal role in virus entry and replication. While some host glycan-based cellular receptors for HPIV-3 have been identified, the dynamics of the host glycome upon HPIV-3 infection has never been studied. Herein, we report the first mass spectrometry-based study that provides direct insight into the remodelling of the human lung adenocarcinoma cell (A549) glycome upon HPIV-3 infection. In this study we observed that HPIV-3 infection led to significant host-cell glycome changes in both oligomannose and sialylated complex-type *N*-glycans. Moreover, notable changes were also observed in both core 1 and core 2 type *O*-glycans, along with distinct glycosphingolipid remodelling in infected cells compared to their mock-infected counterparts. Our study presents the first evidence that hPIV-3 infection alters host-cell glycome, offering new insights into the virus's impact on host cellular processes.

Keywords: respirovirus, host-cell glycome, mass spectrometry, glycome remodelling.

Introduction

Human parainfluenza viruses (HPIVs) are among the most common causes of respiratory tract infections in children under the age of five, the elderly, and immunocompromised individuals, often resulting in high mortality rates[1]. The most common clinical manifestations reported for HPIV infections include colds, croup, bronchiolitis, bronchitis, and pneumonia. HPIV infections account for 40% of paediatric hospitalizations for lower respiratory tract infection and 75% of croup cases across the world, annually[1]. Despite the significant health burden posed by HPIV infections, neither antiviral drugs nor vaccines are currently available. The infection begins in the nose and oropharynx and then spreads to the lower respiratory tract in severe cases, with ciliated epithelial cells of both the upper and lower respiratory tracts being the primary targets of HPIVs[2,3] . There are four major serotypes of HPIV, designated as serotypes 1 through 4. HPIV-3 is the most prevalent HPIV subtype worldwide, including Australia, causing seasonal outbreaks in spring mostly after influenza outbreaks[4]. Regardless of serotypes, cell surface carbohydrates (glycans) play an important role in the life cycle of HPIVs[1]. Glycans, carbohydrate-based biopolymers linked by glycosidic bonds, are present in all living organisms. They play significant roles in biology, including maintaining the cell's physical and structural integrity, contributing to the formation of extracellular matrix, mediating signal transduction, assisting in protein folding, and facilitating infection by pathogens[5]. In particular, glycans play numerous roles in viral pathogenesis, including as host cell receptors for adhesion of the virus particle (e.g. influenza virus)[6], protection of the antigenic epitope of viral glycoproteins from the host immune response (e.g. human immunodeficiency virus)[7], and subversion of the immune response by acting as an antibody decoy (e.g. Lassa virus)[8]. Like influenza viruses, HPIV-3 recognizes sialic acids on the host cell via its haemagglutinin-neuraminidase (HN) protein. The neuraminidase activity of the HN protein enables the virus to remove sialic acid residues from glycoproteins and glycolipids on the host cell surface, thereby aiding the release of new virus particles from the infected host-cell[9]. While the important role of glycans for entry and release of HPIV is known, the dynamics of the host-cell glycome expression upon infection remains to be determined. Recent advancements in chromatographic separation, ionization technologies, and mass spectrometry have substantially improved glycomic analyses, enabling high-throughput and structurally informative characterization of glycan species[10]. Notably, liquid chromatography (LC) employing porous graphitized carbon (PGC) stationary phases, coupled with electrospray ionization tandem mass spectrometry (PGC-LC-ESI-MS/MS), allows for precise separation

62 and identification of glycan structural isomers based on retention time and fragmentation
63 patterns[11]. Using this PGC-LC-ESI-MS/MS workflow, we aimed to delineate the dynamic
64 alterations in the host-cell glycome, including *N*-glycans, *O*-glycans, and glycosphingolipid
65 (GSL) glycans, during HPIV-3 infection in human lung epithelial cells (A549).

66 Our results reveal extensive remodeling of the host-cell glycome following HPIV-3
67 infection at both 24 h and 48 h post-infection. Specifically, we observed a pronounced increase
68 in oligomannose-type *N*-glycans and a concomitant reduction in sialylated complex-type
69 *N*-glycans relative to mock-infected controls. Additionally, HPIV-3 infection induced higher
70 expression of core 1 *O*-glycans alongside reduced levels of core 2 *O*-glycans. These changes
71 in *N*- and *O*-glycan profiles were accompanied by significant alterations in GSL glycan
72 composition. Collectively, our findings demonstrate that HPIV-3 orchestrates substantial
73 glycome remodeling in host cells, providing the first comprehensive characterization of these
74 glycomic shifts and offering new insights into HPIV-3 pathogenesis and potential therapeutic
75 targets.

76 Experimental procedures

77 *Cell culture, virus and infection assays*

78 Human lung adenocarcinoma epithelial cells (A549; ATCC, CCL-185) were
79 maintained in Dulbecco's Modified Eagle Medium (DMEM) (Gibco, Cat. no. 10313021) media
80 supplemented with 5% foetal bovine serum (FBS, Gibco, Cat. no. 10099141), 1%
81 Antibiotic-Antimycotic (100X, Gibco, Cat. no. 15240062), 1% MEM Non-essential Amino
82 Acid (100X, Sigma, Cat. no. M7145), 1% L-Glutamine 200 mM (100X, Gibco, Cat. no.
83 25030081) and incubated at 37 °C in a humidified chamber containing 5% CO_2. Human
84 parainfluenza virus type 3 (HPIV-3 JS), genetically modified to incorporate green fluorescent
85 protein (GFP), was obtained from ViraTree (Product # P323). Virus propagation was performed
86 in Rhesus monkey kidney epithelial (LLC-MK2; ATCC, CCL-7) cells using DMEM media
87 supplemented with 1% Antibiotic-Antimycotic, 1% MEM Non-essential Amino Acid, 1%
88 L-Glutamine ($DMEM_{inf}$) at 35 °C in a humidified chamber containing 5% CO_2. Approximately
89 2 million A549 cells were seeded in a 75 cm^2 flask 48 h prior infection. Cells were washed 2
90 times with phosphate buffer saline (PBS) and 5 times with $DMEM_{inf}$. Cell monolayer was
91 infected with HPIV-3 for 1 h at 35 °C and 5% CO_2, with multiplicity of infection (MOI) of 3
92 in triplicates. The mock-infected control was treated the same way as their infected counterpart

93 except for adding viral inoculum. Both infected and mock-infected cells were incubated for 24
94 h and 48 h at 35 °C in a humidified chamber containing 5% CO_2.

95 *Protein and glycosphingolipid (GSL) extraction*

96 Cell culture media from both infected and mock-infected control were collected and
97 mixed with 5 volumes of ice-cold $(CH_3)_2CO$ (Sigma-Aldrich, Cat no. 650501) before storing
98 at -20 °C overnight to precipitate secreted proteins. Infected and mock-infected cells were first
99 washed four times with PBS to remove any residual media, including viral progeny. The cells
100 were then detached with a scrapper and lysed in 1X cold RIPA lysis buffer (Thermo Fisher,
101 Cat. no. 89900) supplemented with 1X protease inhibitor (Roche, cat. no. 11697498001). The
102 mixture was incubated overnight at 4 °C, followed by sonication for 30 min in an ultrasound
103 sonicator (VEVOR Ultrasonic Cleaner). Proteins and glycosphingolipids from cell lysates were
104 extracted through standard chloroform, methanol, and water extraction method described
105 elsewhere[11]. Briefly, 550 µL of chloroform (Sigma-Aldrich, Cat no. 1.02445) were added to
106 each sample and sonicated for 15 min, followed by addition of 350 µL of methanol (Merck,
107 Cat. no. 1.06035). The cell lysates were incubated at room temperature for 15 min with gentle
108 shaking, followed by centrifugation at 3000 x g for 20 min. Upper phase containing
109 glycosphingolipid were transferred to clean tubes. A mixture of 400 µL of chloroform/methanol
110 (2:1) and 400 µL of methanol/water (1:1) was added to the pellets and vortexed vigorously.
111 The mixture was sonicated again for 15 min followed by centrifugation at 3000 x g for 20 min.
112 Upper phase was collected and added to the previous collected sample. An additional 400 µL
113 methanol/water (1:1) mixture was added to the initial chloroform/methanol (2:1) phase and the
114 separation steps were repeated. Proteins were pelleted, by adding 750 µL methanol to the lower
115 phase, followed by centrifugation at 10000 x g for 20 min. The supernatant containing lipids
116 were combined with previously collected upper aqueous phase and subsequently dried using a
117 speed vac concentrator (Thermo Scientific; Savant SPD131DDA). The protein pellets were
118 air-dried and then resuspended in 100 µL 8 M urea. The secreted protein samples were
119 centrifuged at 5000 x g for 40 min to pellet the proteins. Supernatant was decanted and the
120 protein pellets were resuspended in 100 µL 8 M urea. Bicinchoninic acid (Thermo-Fisher, Cat.
121 no. 23227) assay was performed to quantify the proteins. Proteins were reduced and alkylated
122 by adding dithiothreitol (25 mM final concentration) at 60 °C for 1 h and Iodoacetamide
123 (50 mM final concentration) (Merck, Cat. no. 16125), for 30 min in dark at room temperature.

124 *Release of* N- *and* O-*glycans*

125 The glycomics workflow, including the release, reduction, desalting, and PGC clean-up
126 of *N*-, *O*-, and GSL glycans from protein and lipid samples, was performed according to a
127 previously published protocol[12], unless otherwise stated. Dot blotting of proteins on
128 polyvinylidene fluoride (PVDF) membrane (0.45 µm pore size, Millipore, Cat. no.05317) was
129 performed before the release of *N*-, and *O*-glycans. PVDF membrane was first activated with
130 ethanol (Merck, Cat. no. 459828). Approximately 30 µg of proteins were spotted on the
131 membrane. Protein spots were stained using direct Blue (Sigma-Aldrich, Cat. no. 212407),
132 excised, and transferred to a flat bottom polypropylene 96-well plate (Merck, Cat. no.
133 CLS3364), blocked with 1% (w/v) polyvinylpyrrolidone (Sigma-Aldrich, Cat no. PVP40) in
134 50% (v/v) methanol and washed 3 times with 100 µL ultrapure water (Sigma-Aldrich, Cat no.
135 1.15333). The *N*-glycans were then released using PNGase F (1000 units for each reaction)
136 (New England Biolabs, Cat. no. P0709L) for 16 h at 37 °C. The released *N*-glycans were
137 collected after agitation of the sealed plate on a shaker. The PVDF membrane wells were then
138 washed with 2 × 20 µL of water and collated with previously collected *N*-glycans.
139 Subsequently, 10 µL of 100 mM ammonium acetate (pH 5) was added to the collected
140 *N*-glycans, followed by incubation at room temperature for 1 h. The samples were then dried
141 under vacuum and kept in the freezer until further use.

142 To release the *O*-glycans from the same PVDF membrane spot, 2.5 µL of methanol was
143 added to each spot to pre-wet them. About 50 µL 0.5 M sodium borohydride in 100 mM
144 potassium hydroxide was added in each well and the plate was sealed with parafilm to prevent
145 evaporation. Then the plate was incubated for 18 h at 50 °C. The reaction was neutralized with
146 5 µL glacial acetic acid.

147 *Purification and enzymatic release of GSL glycans*

148 Purification of GSLs was performed according to a previously described method[13]. In
149 brief, the dried aqueous and lipid-containing phases were resuspended in 100 µL of methanol
150 for 30 min on a shaker, followed by the addition of 100 µL of water. Then, the sample was
151 loaded onto a tC18 RP cartridge (Waters, Cat. no. WAT036820), that was preconditioned with
152 1 mL of chloroform/methanol (2:1; v/v), 1 mL of methanol and 2 mL of methanol/water (1:1;
153 v/v). After the addition of the sample, the cartridge was washed with 2 mL of methanol/water
154 and the elution was performed with 2 mL of methanol and 2 mL of chloroform and methanol
155 (2:1; v/v). The combined eluate was dried under vacuum and stored at -20 °C until further use.
156 The enzymatic release of the GSL head group was performed by following manufacturer's

157 instructions (New England Biolabs, Cat. no. P0773S). In brief, the dried GSLs were
158 resuspended in 36 µL of WATER, 4 µL of EGCase I reaction buffer and 2 µL of EGCase I
159 enzyme. The reaction mixture was then incubated at 37 °C for 36 h. The separation and
160 purification of the released glycans from the were performed on tC18 RP cartridge, which was
161 preconditioned with 2 mL of methanol and 2 mL of water. After loading the sample, the
162 cartridge was washed twice with 200 µL of water. The flowthrough containing the released
163 glycans, along with the column washes, was collected and dried under vacuum.

164 *Reduction of* N-*glycans and GSL glycans*

165 The Glycans were reduced by adding 25 µL of 1 M $NaBH_4$ (Sigma-Aldrich, Cat. no.
166 213462) in 100 mM potassium hydroxide (Sigma-Aldrich, Cat. no. 757551), through
167 incubation at 50 °C for 3 h. Three microliters of glacial acetic acid (Merck, Cat. no.
168 5.33001.0050) was added to quench the reaction.

169 *Desalting of reduced glycans*

170 Reduced *N*-, *O*-, and GSL glycans were desalted using cation exchange. The columns
171 were self-packed with 25 µL of strong cation-exchange resin (50W-X8) slurry (BIO-RAD, cat.
172 no. 1421451) in Methanol onto a ZipTip C_{18} resin tip. The columns were preconditioned
173 sequentially with 3 × 50 µL of 1 M HCl (Sigma-Aldrich, cat. no. 320331), 3 × 50 µL of
174 methanol, and 3 × 50 µL of ultrapure water. The samples were applied to the preconditioned
175 columns, and the original sample tube was rinsed with 50 µL of ultrapure water, which was
176 then added to the column. The glycans were subsequently eluted with 2 × 50 µL aliquots of
177 ultrapure water. The eluted glycans were then dried and treated with 4 × 100 µL of methanol
178 to remove the borate salt.

179 *PGC clean-up of* N-*,* O- *and* GSL *glycans*

180 Carbon material was removed from the carbograph SPE cartridge (BGB Analytik AG,
181 cat. no. SPU-5122423) and a slurry was prepared with a concentration of 50 mg/mL in
182 methanol. About 25 µL of the slurry was loaded into a ZipTip with 0.6 µL C18 resin. The
183 columns were pre-conditioned with 3 × 50 µL of 0.1% trifluoroacetic acid (Sigma-Aldrich, cat.
184 no. 302031) and 3 × 50 µL of 90% acetonitrile (Sigma-Aldrich, cat. no. 1.00029), 0.1%
185 trifluoroacetic acid. The glycan samples were loaded in 50 µL of 0.1% trifluoroacetic acid.
186 Finally, the samples were eluted with 50 µL of 50% acetonitrile, 0.1% trifluoroacetic acid. The

187 eluted glycans were then dried using a speed vac concentrator (Thermo Scientific; Savant
188 SPD131DDA) and stored at -20 °C until further use.

189

190 *PGC-LC-ESI-MS/MS of released* N- *and* O- *and GSL glycans*

191 The PGC-LC-ESI-MS/MS glycomics analysis was performed using an amaZon speed
192 ion trap (IT-MS, Bruker, Bremen, Germany) linked to an Ultimate 3000 UHPLC system
193 (Dionex/Thermo). Five microliters of glycan sample were injected by the autosampler and
194 separated using an analytical PGC column (Hypercarb™ PGC Column, Thermo Fisher
195 Scientific, 3 µm particle size, inner diameter 1 mm x 30 mm, maintained at 45 °C). Ten
196 millimolar ammonium bicarbonate was used as buffer A and 70% acetonitrile in 10 mM
197 ammonium bicarbonate was used as solvent B in the mobile phase. The flow rate was set at 15
198 µL/min for *N*-, *O*-, and GSL glycans. The gradient system used to separate the *N*-glycans was
199 as follows: 1% B at 0 min; 14% B at 6 min; 25% B at 25 min; 70% B at 45 min; 98% B at 50
200 min; 1% B at 51 min; 1% B at 65 min. *O*- and GSL glycans were separated using the following
201 gradient: 1% B at 0 min; 25% B at 25 min; 70% B at 45 min; 98% B at 47 min; 1% B at 51
202 min; 1% B at 65 min. Eluted glycans were then ionised using ESI in negative ion mode and
203 detected with an ion-trap mass analyser. A *m/z* range of 460–1,800 was set for data-dependent
204 precursor scanning. The collision induced dissociation (CID) fragmentation was used as the
205 fragmentation method where the five most intense precursors of each MS scan were selected
206 for tandem MS. Capillary voltage was set at 3.3 kV, with nitrogen drying gas flow rate 6 L/min
207 at 8.70 psi nebulizer pressure. An ICC target of 70,000 and maximum accumulation time of
208 100 ms were used. Smart parameter setting (SPS) was set to 1200 *m/z*.

209 *Glycan structure determination and relative quantitation*

210 The MS data was manually analysed using Compass Data analysis version 4.4 (Bruker
211 Daltonics) and then quantitated with Skyline version 22.2[14]. Monosaccharide compositions
212 were determined using the Glycomod tool available on the Expasy[15] with a mass tolerance of
213 0.5 Da. The glycan structures were assigned manually from the tandem mass spectra and
214 characterized with the GlycoWorkbench version 2.1[16]. The fragmentation spectra were also
215 further matched with UniCarb KB to confirm all the structures[17]. Normalised relative
216 intensities of individual glycan structures were calculated in Microsoft Excel and using
217 GraphPad Prism, and to perform statistical analysis

218 *Statistical analysis*

219 All the experiments were done in triplicates, and statistical analysis was performed in
220 GraphPad Prism (version 9). *P* values were calculated by performing an unpaired two-tailed
221 Welch's *t*-test at 95% confidence level. Data visualization was performed in R Studio, with
222 final figure preparation and refinement done in Adobe Illustrator.

223 *Glycan Representation*

224 Glycan structures were visualized by cartoons generated using GlycoWorkbench
225 Glycans were depicted according to the SNFG (Symbol Nomenclature for Glycans) notation:
226 *N*-acetylglucosamine (*N*; blue square), fucose (F; red triangle), mannose (H; green circle),
227 galactose (H; yellow circle), *N*-acetylneuraminic acid (S; purple diamond), and
228 *N*-glycolylneuraminic acid (G; light blue diamond).

229 **Results**

230 *HPIV-3 infection triggers significant changes in* N-*glycan expression in the host cell*

231 We hypothesized that viral infection could alter glycan expression in host cells, which
232 may influence processes such as progeny virion release, cell-cell and cell-matrix interactions,
233 and overall cell signalling. To study the impact of infection on host-cell glycosylation, we
234 analysed *N*-glycan expression of cell-extracted and secreted proteins from both mock-infected
235 and HPIV-3 infected A549 cells, at 24 h and 48 h timepoints post-infection. In total, 70
236 *N*-glycan species (including structural and compositional isomers) were observed across
237 infected and mock-infected cells, varying from 5 to 17 monosaccharides (Table S1). The glycan
238 species were manually interpreted and validated based on the existence of specific fragment
239 ions in their MS/MS spectra[18]. The identified *N*-glycans were grouped based on structural
240 features (oligomannose, complex sialylated, complex neutral, hybrid, and paucimannose).
241 Relative abundances of each glycan species from infected and mock-infected cells were
242 statistically analysed (Table S2). The differential expression of *N*-glycans in infected and
243 mock-infected cells is provided in Figure 1a-c.

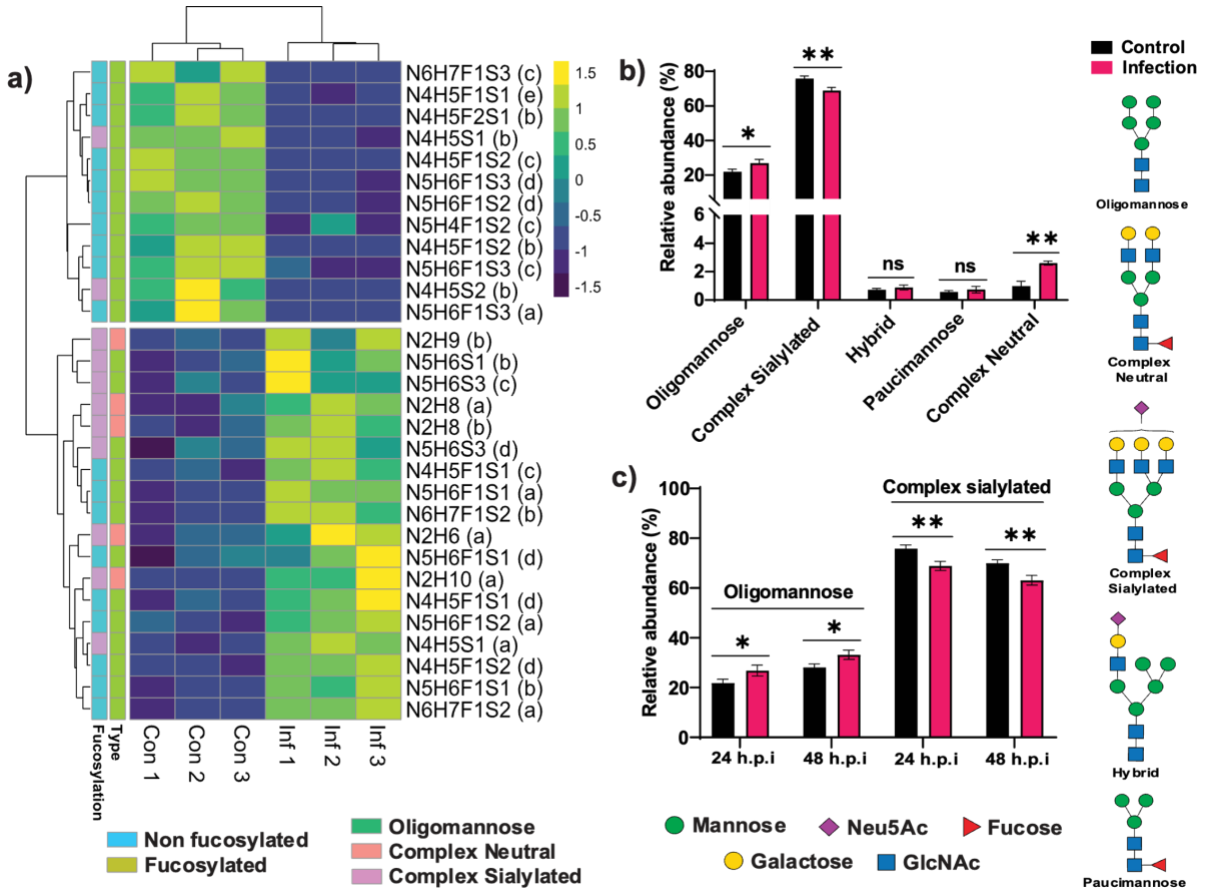

Figure 1: ***HPIV-3 infection modulates expression of* N*-glycans on cell-extracted proteins.*** *a) Heatmap representing the relative abundance of significantly altered* N*-glycans before and 24 h post-infection. b) Differential expression of all major types of* N*-glycans on infected and mock-infected cells at 24 h post-infection. c) Altered expression of oligomannose-type and sialylated complex-type* N*-glycans at 24 h and 48 h timepoints post-infection. n=3, *P<0.05, **P<0.01, ns: not significant, unpaired Welch's t-test. N:* N*-acetylhexosamine; H: Hexose; F: Fucose; S:* N*-acetylneuraminic Acid; h.p.i: hours post-infection.*

In the context of total *N*-glycan composition, we observed that sialylated complex-type *N*-glycans and oligomannose-type glycans were the most abundant, comprising more than 90% of total *N*-glycans detected in both mock-infected and HPIV-3 infected A549 cells (Table S2). We observed a significantly higher expression of oligomannose-type *N*-glycans (from 21.87% ± 1.50% in mock-infected to 26.87% ± 2.18% in infected cells) at 24 h post-infection (Figure 1b). We also observed diverse sialylated structures ranging from mono-sialylated biantennary to tri-sialylated tri-antennary complex glycans (Table S1). HPIV-3 infection resulted in significant reduction of sialylated complex-type *N*-glycans in infected cells, decreasing from 75.85% ± 1.47% in mock-infected to 68.90% ± 1.81% in infected cells (Figure 1b). To identify if the altered expression of glycans in infected cells is stable, we analysed the glycan expression also at 48 h post-infection. Notably, similar changes in both oligomannose-type and sialylated complex-type *N*-glycans were also observed at 48 h post-infection. For example, an approximately 5% increase in oligomannose-type and a 7% decrease in sialylated

complex-type *N*-glycans were detected in infected cells (Figure 1c). Moreover, we saw a subtle, yet statistically significant, increase (~1.5%) in the expression of complex neutral-type *N*-glycans upon 24 h and 48 h post-infection. Two other major glycan types, hybrid and paucimannose, remained unchanged during infection at 24 h and 48 h.

Cell secreted proteins play important roles in maintaining cell communication and signalling, and glycans that decorate these secreted proteins are key to these interactions[19]. Considering these important roles, we analysed the glycans released from secreted proteins of both infected and mock-infected cells and compared their relative abundances (Figure 2a).

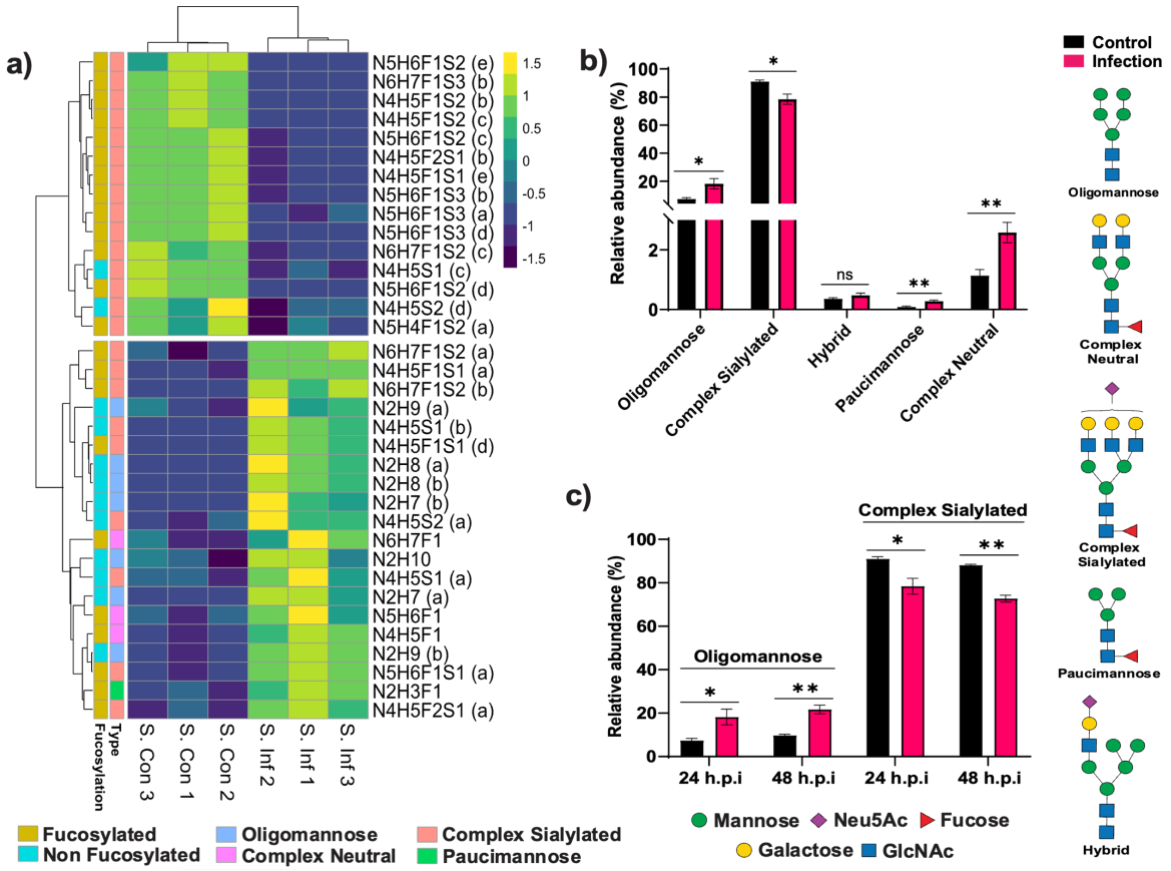

Figure 2: ***HPIV-3 infection modulates expression of* N*-glycans on secreted proteins.*** *a) Heatmap represents the relative abundance of significantly altered* N*-glycans before and at 24 h post-infection. b) Differential expression of all major types of* N*-glycans in infected and mock-infected cells at 24 h post-infection. c) Altered expression of oligomannose-type and sialylated complex-type* N*-glycans at 24 h and 48 h post-infection. n=3, *P<0.05, **P<0.01, ns: not significant, unpaired Welch's t-test. N:* N*-acetylhexosamine; H: Hexose; F: Fucose; S:* N*-acetylneuraminic Acid; h.p.i: hours post-infection.*

The *N*-glycome composition of secreted proteins differed slightly from that of cell-extracted proteins. Approximately 90% of *N*-glycans on secreted proteins were processed from oligomannose to sialylated complex-type structures, whereas cell-extracted proteins contained about 70-74% sialylated complex-type *N*-glycans (Table S1). However, in agreement with *N*-glycans on cellular proteins, expression of sialylated complex-type glycans was decreased

283 from 91% ± 1.08% in mock-infected control to 78.44% ± 3.66% in HPIV-3 infected cells (24
284 h post-infection). We also observed a significant increase of ~11% in oligomannose-type
285 glycans in response to viral infection (24 h post-infection) (Figure 2b). Notably, these changes
286 were nearly twice as pronounced as those observed in cell-extracted proteins, which showed a
287 7% decrease in sialylated complex-type and a 5% increase in oligomannose-type *N*-glycans.
288 Likewise, HPIV-3 infection also modulated the *N*-glycome composition of secreted proteins at
289 48 h post-infection. The level of oligomannose-type glycans was augmented by more than 12%,
290 whereas the expression of sialylated complex-type *N*-glycans was reduced by more than 15%
291 on secreted proteins collected from HPIV-3 infected cells compared to mock-infected control
292 (Figure 2c). The complex neutral type comprised of 1% to 2% of the total secreted protein
293 *N*-glycome in mock-infected cells. However, the expression of this glycan type was observed
294 to be doubled at both 24 h and 48 h post-infection (Figure 2b). There were no significant
295 changes observed in relative intensities of hybrid and paucimannose-type *N*-glycans on
296 secreted proteins after infection irrespective of the time points (Figure 2b).

297 *Differential expression of oligomannose and sialylated complex-type* N-*Glycans at the*
298 *individual glycan level*

299 Next, we examined whether changes in oligomannose and sialylated complex-type
300 *N*-glycans followed a similar pattern at the level of individual glycan species. A detailed
301 analysis enabled us to identify that, although overall abundance of oligomannose-type
302 *N*-glycans increased from the mock-infected control (21.87% ± 1.50%) to infected cells
303 (26.87% ± 2.18%), not all oligomannose species exhibited a similar trend. We observed that
304 individual oligomannose species were either increased or remained constant post-infection
305 (Figure S1, S2). Oligomannose glycans containing 5 to 9 mannose units were identified across
306 infected and mock-infected cells. Of these, both isomers of N2H8, one isomer of N2H9, N2H6,
307 N2H7 and N2H10 were increased at 24 h post-infection on cell-extracted proteins (Figure S1a).
308 Likewise, each isomer of N2H7 to N2H9 was upregulated, whereas others remained constant
309 after 48 h of infection when compared to the mock-infected control (Figure S2a). This trend
310 was consistent for secreted proteins both at 24 h and 48 h post-infection, as at least one isomer
311 from N2H6 to N2H9 was significantly elevated (Figure S1b & S2b). We also detected a range
312 of sialylated structures, from mono-sialylated bi-antennary to tri-sialylated tri-antennary
313 complex-type *N*-glycans, on both cell-extracted and secreted proteins. Using a
314 PGC-LC-ESI-MS/MS workflow to enable the separation of isomers based on their
315 corresponding retention time, we found that the majority of the sialylated structures displayed

316 multiple isomeric forms (Table S1). Overall, there was an approximately 7% reduction in
317 sialylated complex-type *N*-glycans in infected cells compared to their mock-infected
318 counterparts on the cell-extracted proteins. However, this overall decrease did not apply
319 uniformly to all sialylated complex-type *N*-glycan species, as some were downregulated while
320 others were either upregulated or remained unchanged in infected cells (Figure S3 to S8). For
321 example, singly sialylated bi-antennary structures with (N4H5F1S1) and without core fucose
322 (N4H5S1), along with some doubly, triply sialylated bi-antennary (N4H5F1S2) and
323 tri-antennary (N5H6S3) structures were found to be upregulated in infected cells (Figure S3).
324 On the other hand, structural isomers of the singly sialylated bi-antennary structures with the
325 composition of N4HS5F1S1, along with doubly and triply sialylated bi-antennary (N4H5F1S2)
326 and tri-antennary (N5H6F1S3) *N*-glycans were downregulated upon HPIV-3 infection (Figure
327 S4). These diverse changes in the expression of sialylated complex-type *N*-glycans were
328 detected across cell-extracted and secreted proteins, regardless of post-infection time points
329 (Figure S5-S10). Together, these findings highlight that HPIV-3 infection results in selective
330 remodelling of both oligomannose and sialylated complex-type *N*-glycans, with distinct
331 changes observed at the level of individual glycan species.

332 *HPIV-3 infection modulates expression of sialic acid isomers on* N-*glycans*

333 HPIV-3 binds to sialylated glyco-epitopes on host cells via its HN protein to initiate
334 infection and later uses the same protein's neuraminidase activity to cleave sialic acids
335 (Neu5Ac), enabling the release of newly formed virions[20]. Considering this, we hypothesize
336 that HPIV-3 infection could directly affect the expressions of glycans terminating in Neu5Ac.
337 Structural isomers of sialylated complex-type *N*-glycan species arise from the linkage of
338 Neu5Ac to the terminal galactose via either an α2,3 or α2,6 glycosidic bonds on each antenna
339 of the glycan. Previous studies suggest that α2,3- and α2,6-linked Neu5Ac residues on
340 galactose serve as receptors for HPIV-3, with the viral HN neuraminidase showing a preference
341 for α2,3-linked Neu5Ac-containing glycans over their α2,6-linked counterparts[20]. Such
342 differential recognition and cleavage specificity suggest that HPIV-3 may selectively modulate
343 sialylation patterns during infection. Although sialic acid linkage isomers can be definitively
344 characterized using linkage-specific neuraminidases, the linkage of structurally simple glycans
345 bearing a single sialic acid residue can also be inferred based on their retention behaviour on
346 PGC column, as demonstrated in previously published studies[21,22]. We observed three potential
347 isomers of bi-antennary complex *N*-glycans with *m/z* 965.8^{2-} (N4H5S1). In agreement with
348 previous studies, the first two structures eluting closely on the PGC column are arm isomers of

349 an α2,6-linked mono-sialylated complex-type *N*-glycan, whereas the third structure, eluting 6
350 minutes later than the first two, represents an α2,3-linked isomer of the same composition
351 (N4H5S1)[22]. Comparing the relative abundance of these species, we found that HPIV-3
352 infection results in a significantly lower expression of the α2,3-linked isomer in both
353 cell-extracted and secreted proteins, irrespective of post-infection time points (Figure 3a & 3b).
354 On the other hand, the α2,6-linked isomer of the same *N*-glycan composition was increased in
355 infected cells when compared to the mock-infected control (Figure 3c & 3d).

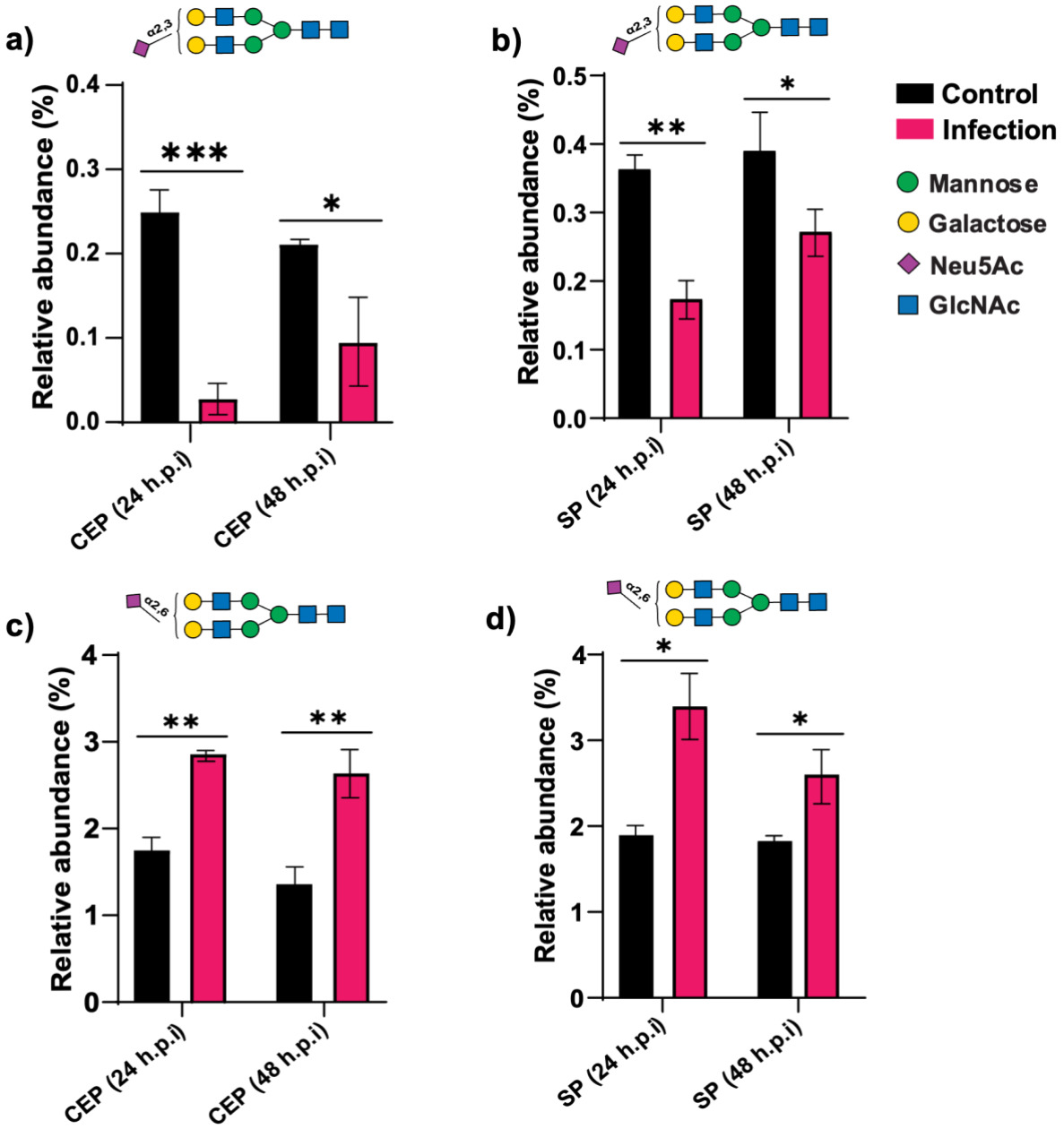

356

357 *Figure 3:* ***Differential expression of α2,3- and α2,6-linked isomers of mono-sialylated complex-type N-glycan (N4H2S1) in***
358 ***infected vs. mock-infected cells:*** *(a) α2,3 on cell-extracted proteins, (b) α2,3 on secreted proteins, (c) α2,6 on cell-extracted*
359 *proteins, (d) α2,6 on secreted proteins at 24 h and 48 h post-infection. n=3, *P<0.05, **P<0.01, ***P<0.001, unpaired*
360 *Welch's t-test. CEP: Cell extracted proteins; SP: Secreted proteins. h.p.i: hours post-infection.*

361 *Alterations in* O*-glycan profiles induced by HPIV-3 infection*

362 Since we identified significant modulation of the host-cell *N*-glycome upon HPIV-3
363 infection, we pondered if the *O*-glycome of host cell could also be altered. Like *N*-glycans,
364 *O*-glycans also have a wide range of roles in the viral replication cycle, such as facilitating viral
365 entry by acting as co-receptors and regulating viral navigation at the cell surface to assist virion
366 progeny egress[23]. Changes in the *O*-glycan profile because of HPIV-3 infection could
367 significantly affect the diverse and multifaceted functions mediated by *O*-glycans. To address
368 this open question, we investigated *O*-glycan expression at 24 h and 48 h timepoints
369 post-infection in both cell-extracted and secreted proteins. The profiling of *O*-glycans was
370 carried out essentially as described for the *N*-glycans. In total, 9 *O*-glycans structures including
371 structural isomers were detected in cell-extracted proteins from infected and mock-infected
372 A549 cells (Table S1). The *O*-glycome of A549 cell is comprised of core 1 and core 2 type
373 glycans with core 2 type the most abundant (from 67% to 93% across mock-infected and
374 infected cells) (Table S2). A distinctive *O*-glycan profile was found on infected cell-extracted
375 proteins when compared to their mock-infected counterpart (Figure 4).

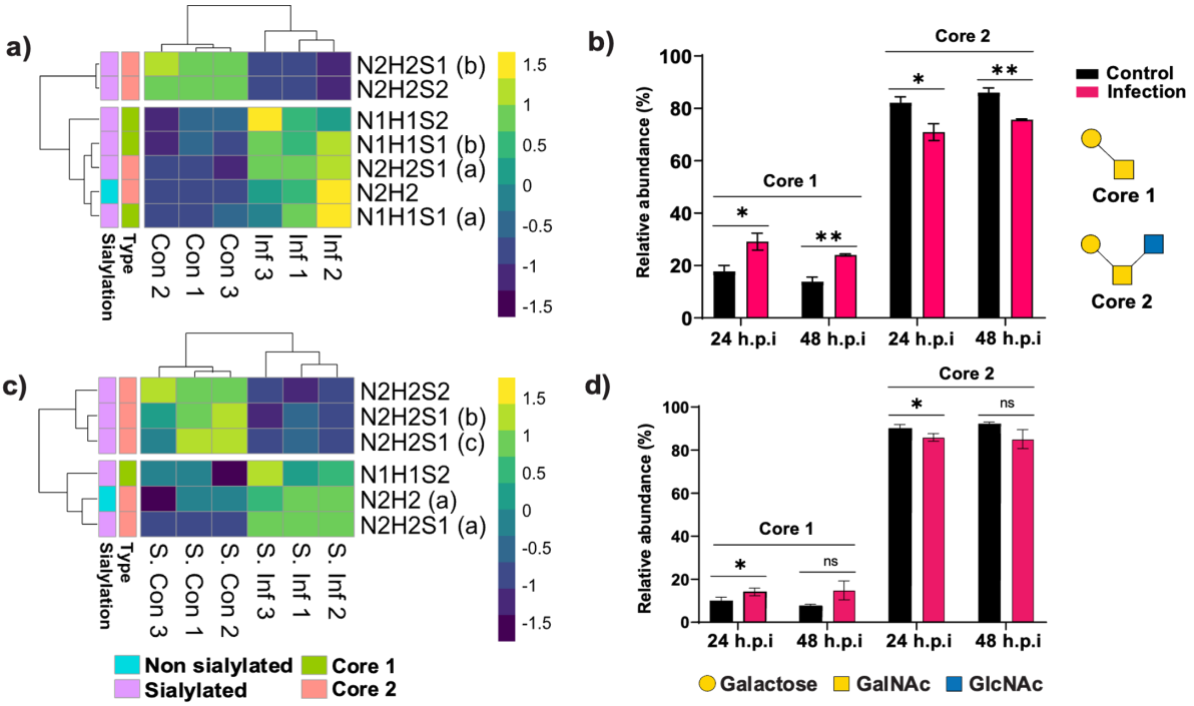

376

377 *Figure 4:* ***HPIV-3 infection modulates expression of* O*-glycans on cell-extracted and secreted proteins.*** *a) Heatmap*
378 *represents the relative abundance of significantly altered* O*-glycan species on cell-extracted proteins before and 24 h after*
379 *infection. b) Differential expression of two major core types on cell-extracted proteins at 24 h and 48 h post-infection. c)*
380 *Heatmap represents the significantly altered* O*-glycan species on secreted proteins before and 24 h post-infection. d)*
381 *Differential expression of two major core types on secreted proteins at 24 h and 48 h post-infection. n=3, *P<0.05, **P<0.01,*
382 ****P<0.001, ns: not significant, unpaired Welch's t-test. N:* N*-acetylhexosamine; H: Hexose; F: Fucose; S:*
383 N*-acetylneuraminic Acid; h.p.i: hours post-infection.*

384 We observed that core 2 type *O*-glycans from host cell-extracted proteins were downregulated
385 upon HPIV-3 infection at 24 h post-infection timepoint, reducing from 82.17% ± 2.20% in
386 mock-infected cells to 70.90% ± 3.23% in infected cells (Figure 4b). Moreover, the
387 downregulation of the core 2 type was compensated by an approximately 12% increase of
388 core 1 type in infected cells. A similar response was observed at 48 h post-infection. Next, we
389 sought to determine if the expression of *O*-glycans on secreted protein are also altered upon
390 HPIV-3 infection. A moderate decrease, from 90.10% ± 1.78% in mock-infected to
391 85.91% ± 1.78% in infected cells, of secreted protein core 2 type glycans and a corresponding
392 increase, from 9.93% ± 1.78% in mock-infected to 14.10% ± 1.77% in infected cells, of
393 secreted protein core 1 type glycans was found at 24 h timepoint post-infection (Figure 4d).
394 The same trend was found at 48 h timepoint post-infection (Figure 4d).

395 Interestingly, upon investigating individual *O*-glycan species, we observed a similar
396 pattern of infection-induced alterations across cell-extracted and secreted proteins irrespective
397 of post-infection time points. For example, the expression of the di-sialylated core 2 species on
398 cell-extracted proteins, characterized by an *m/z* of 665.2^{2-} (composed of N2H2S2), was reduced
399 by approximately three-fold, with a ~27% and 47% decrease at the 24 h and 48 h timepoints
400 post-infection, respectively in infected cells (Figure 5a and 5b). In contrast, the mono-sialylated
401 core 2 glycan [N2H2S1(a)] showed a remarkable increase in expression of ~26% and 37% at
402 24 h and 48 h timepoints post-infection, respectively upon infection (Figure 5a and 5b).

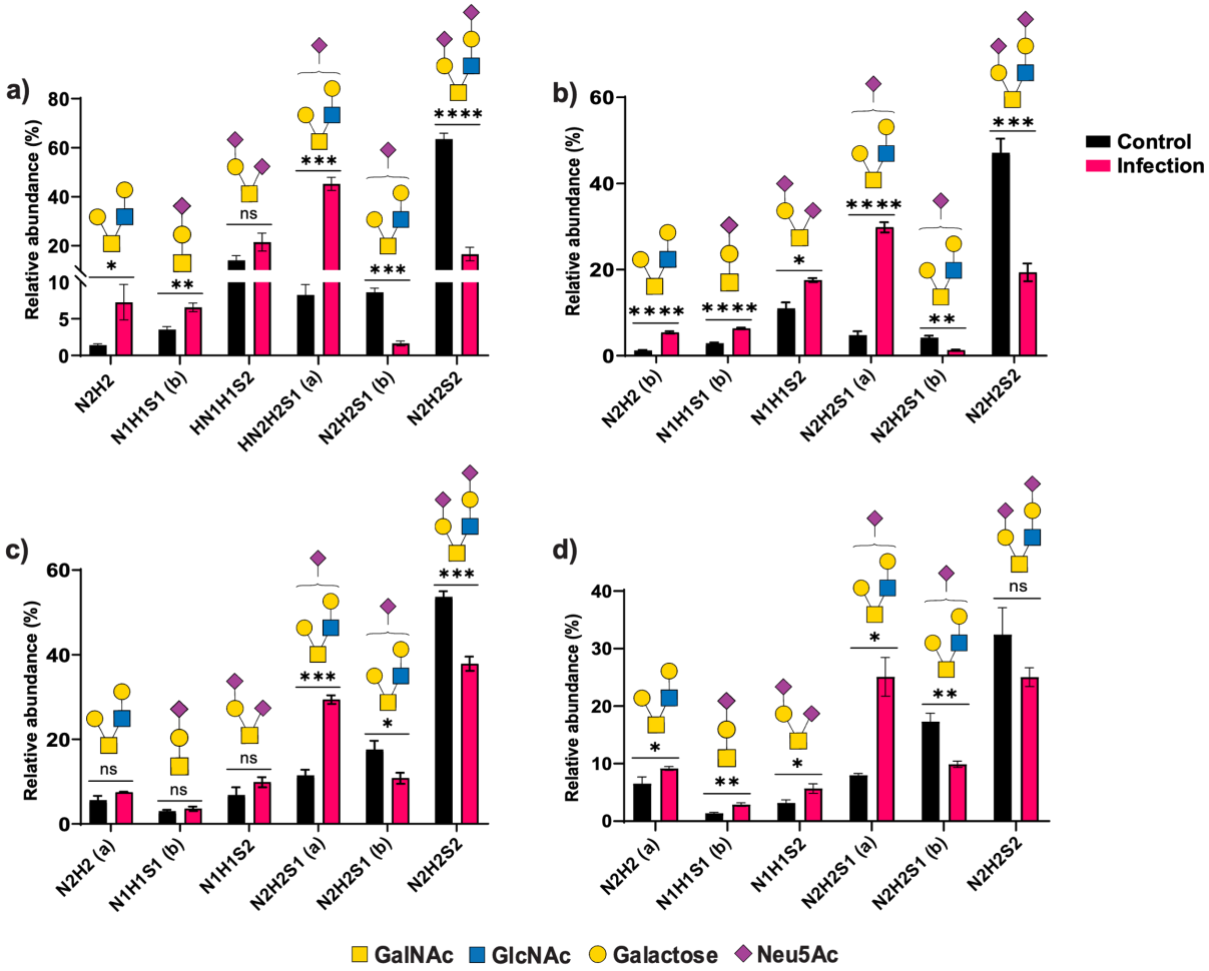

Figure 5: ***HPIV-3 triggers modulated O-glycan expression in infected and mock-infected cells.*** *Relative abundance of all the significantly altered O-glycan species on cell-extracted proteins at a) 24 h, and b) 48 h post-infection. Relative abundance of all the significantly altered O-glycan species on secreted protein at c) 24 h, and d) 48 h post-infection. n=3, *P<0.05, **P<0.01, ***P<0.001, ns: not significant, unpaired Welch's t-test. N: N-acetylhexosamine; H: Hexose; S: N-acetylneuraminic Acid.*

This trend was similarly observed for secreted proteins, independent of the post-infection timepoint (Figure 5c and 5d). Moreover, a structural isomer of the same composition [N2H2S1(b)] was reduced upon infection across cell-extracted and secreted proteins (Figure 5a-d). Interestingly, a core 1 type doubly-sialylated *O*-glycan, with a composition of N1H1S2, was found to be significantly elevated in infected cells for both cell-extracted and secreted proteins at each post-infection timepoint (Figure 5a-d). We observed a slightly favourable expression of core 1 type *O*-glycans compared to core 2 type, along with altered expression of glycans carrying specific sialylated glyco-motifs in response to infection. These changes were consistent for glycans released from both cell-extracted and secreted proteins, regardless of post-infection time points.

420 *HPIV-3 infection induces remodelling of glycosphingolipid (GSL)-associated glycans*

421 GSL glycans represent a significant portion of the host glycome and are primarily
422 located on the cellular plasma membrane, where their sugar moieties are exposed to the external
423 environment[14]. These glycans are involved in various biological processes, including
424 infections[24]. Some viruses (e.g HPIV-3[20], HIV[25], Polyomavirus[26]) are historically known to
425 utilize GSL glycans in their life cycle. However, no studies have reported host cell GSL glycan
426 dynamics in response to parainfluenza viral infection. To characterize GSL glycans, GSLs were
427 extracted from both infected and mock-infected cells before the enzymatic release of the
428 glycans from the head groups, which were then analysed by PGC-LC-ESI-MS/MS. In total, 12
429 GSL glycan species were detected, and the relative intensities of each glycan species were
430 compared between infected and mock-infected control (Table S1). The structure of some of the
431 GSL glycans could only be partially resolved in this study due to the absence of informative
432 fragment ions in tandem MS, and the lack of *exo*-glycosidase digestion in our study. Therefore,
433 there were no GSL glycans class wide comparison made between infected and mock-infected
434 controls. However, major alterations have been detected at the individual glycan level in
435 infected cells (Figure 6).

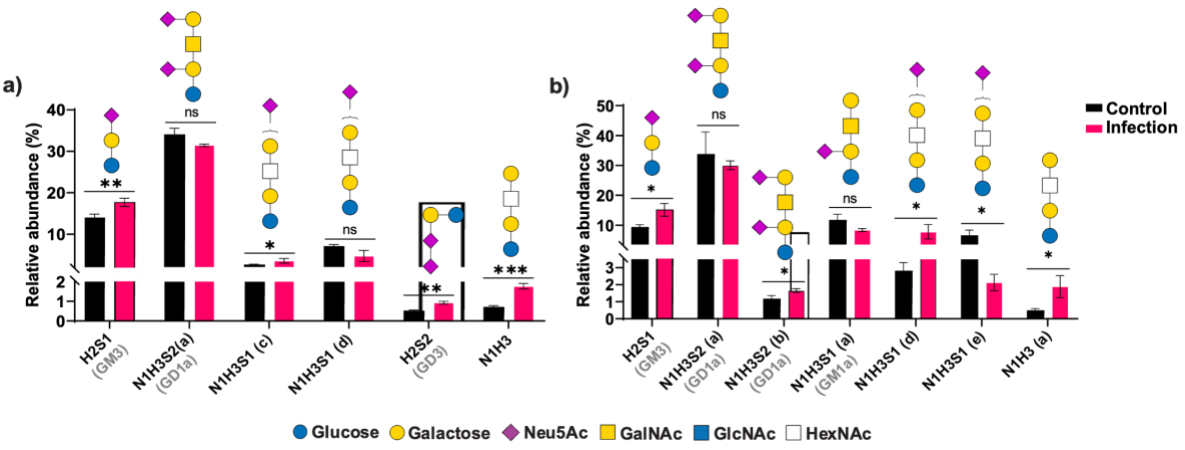

436

437 *Figure 6:* ***HPIV-3 infection triggers altered expression of GSL glycans.*** *Relative expression of all the significantly altered*
438 *GSL glycan species at a) 24 h, and b) 48 h post-infection. n=3, *P<0.05, **P<0.01, ***P<0.001, ns: not significant, unpaired*
439 *Welch's t-test. N:* N-*acetylhexosamine; H: Hexose; S:* N-*acetylneuraminic Acid.*

440 Gangliosides containing one and two Neu5Ac residues were the most abundant GSL glycan
441 types in A549 cells followed by the neo(lacto)-series. The GSL glycan, comprised of H2S1
442 (GM3), appeared to be increased in expression from 14.0% ± 0.84% in mock-infected cells to
443 17.66% ± 1.01% in infected cells, 24 h post-infection (Figure 6a). The increased expression of
444 GM3 remained stable even at 48 h timepoint post-infection (Figure 6b). Another ganglioside

445 comprised of N1H3S2 (GD1a), the most abundant GSL glycan in A549 cells, was reduced in
446 expression from 34.02% ± 1.57% in mock-infected cells to 31.44% ± 0.27% in infected cells,
447 at 24 h timepoint post-infection. A similar trend was observed at 48 h timepoint post-infection
448 despite the change not being statistically significant. Additionally, several other GSL glycan
449 species were also observed to be altered in response to HPIV-3 infection. Two partially resolved
450 isomers with the composition of H3N1S1 (presumably sialylated neo(lacto)-series or GM1
451 gangliosides) showed an opposite trend to each other upon infection. The changes were more
452 prominent at 48 h timepoint post-infection when compared to the mock-infected control.
453 Interestingly, a previous study reported that the sialylated neo(lacto)-series, with the same
454 composition, is recognised by HPIV-3 using a solid-phase binding assay[20]. Higher expression
455 of one of the H3N1S1 isomers in infected cells could be attributed to the reduced expression
456 of GD1 (H3N1S2), as HPIV-3 HN mediated sialic acid cleavage from GD1 glycan would
457 potentially generate a glycan with the composition of H3N1S1, thereby contributing to overall
458 increase of that species upon infection. Furthermore, the expression of GD3 (H2S2) was found
459 to be elevated only at 24 h timepoint post-infection and no significant change was observed at
460 48 h timepoint post-infection. A precursor glycan, belonging to either gangliosides or
461 neo(lacto)-series, with composition of H3N1 was found to be elevated at both 24 h and 48 h
462 timepoints post-infection.

463 **Discussion**

464 Every cell in nature is decorated with a dense layer of carbohydrates (glycans)
465 covalently linked to proteins or lipids, forming the glycocalyx. These glycans form the
466 foundation of a universal biological language known as the glycome, playing active roles in
467 numerous cellular processes[27]. However, microorganisms such as viruses exploit these cell
468 surface resident glycans by using them as receptors or co-receptors[28]. Additionally, viruses take
469 advantage of the host-cell glyco-machinery to decorate their own surface proteins with glycans,
470 acting as protective shields to evade the host immune response[29,30]. During human evolution,
471 viruses along with other pathogens such as bacteria and parasites have co-evolved with their
472 human host and consequently have actively participated in the remodelling of the human cell
473 glycome[31]. For instance, it is widely accepted that evolutionary pressure from pathogens played
474 a significant role in the loss of certain carbohydrates, such as *N*-glycolylneuraminic acid
475 (Neu5Gc) and α-Gal, in human[32,33].

476 To date, only a few studies have described the changes in host-cell glycosylation upon
477 viral infection and the role of an altered glycome expression in triggering innate immune
478 response[6,34,35]. For example, a lectin microarray based study has suggested a significant
479 increase of oligomannose-type glycans in ferret lung upon influenza virus infection, which was
480 further found to be associated with disease severity[6]. More recently, several studies on
481 SARS-CoV-2 infection observed an altered glycosylation profile on antibodies against the viral
482 spike protein with lower fucosylation and sialylation, that ultimately affects the effector
483 functions of antibodies[34,35]. However, these studies either did not employ more sensitive
484 techniques like mass spectrometry or focused solely on the glycosylation of antibody (IgG)
485 against viral protein, rather than examining the glycosylation of infected host-cells. To the best
486 of our knowledge, there is no reported study on the host-cell glycome response to HPIV-3
487 infection. Thus, we employed a highly sensitive mass spectrometry technique coupled with
488 porous graphitized carbon liquid chromatography to reveal the global glycosylation (*N*-, *O*- and
489 GSL glycans) changes of HPIV-3-infected cells. Our analysis revealed an approximately 5%
490 to 12% increase of oligomannose-type *N*-glycans on cell-extracted and secreted proteins, both
491 at 24 h and 48 h post-infection timepoints. This increase may reflect a host cellular response to
492 infection-induced activation of the unfolded protein response (UPR), as has been proposed in
493 other viral systems, such as influenza infection in the ferret lung[6]. The UPR is a
494 well-characterized cellular stress mechanism that is activated when unfolded or misfolded
495 proteins accumulate in the endoplasmic reticulum (ER), disrupting protein homeostasis[36]. In
496 response, the cell initiates UPR signalling to restore ER function by enhancing the folding
497 capacity of the ER, reducing protein translation, and promoting the degradation of misfolded
498 proteins[36]. One important hallmark of UPR activation is the increase in oligomannose-type
499 *N*-glycans, which are essential intermediates in the early stages of protein glycosylation and
500 folding[6,37]. These glycans are particularly important for the quality control of nascent
501 glycoproteins, as they interact with ER-resident chaperones such as calnexin and calreticulin[37].
502 This interaction ensures that only properly folded proteins proceed along the secretory pathway,
503 while misfolded proteins are retained and targeted for ER-associated degradation (ERAD)[32].
504 In the context of HPIV-3 infection, we observe an increase in oligomannose-type glycans which
505 may reflect a host-cellular response to the stress placed on the ER to fold both viral and cellular
506 proteins. Viral infection frequently disrupts ER homeostasis, not only due to synthesis of viral
507 proteins but also through inflammation-induced oxidative stress and altered calcium
508 signalling[38,39]. As a result, the host cell may ramp up UPR signalling to maintain protein
509 homeostasis, not only for its own proteins such as membrane receptors, transporters, or

510 immune-modulatory proteins, which are critical for cellular survival and antiviral responses,
511 but also for the proper folding and processing of viral proteins[40,41]. Together, our findings
512 support the hypothesis that the increased abundance of oligomannose-type *N*-glycans is driven
513 by UPR-mediated adaptation aimed at preserving ER function and protein quality control
514 during HPIV-3 infection. However, direct evidence for UPR activation in our system is still
515 lacking. Future studies employing transcriptomics or proteomics analysis, particularly
516 monitoring UPR markers such as BiP/GRP78, CHOP, and XBP1 splicing, will be essential to
517 confirm whether the UPR pathway is indeed engaged in HPIV-3-infected cells and driving the
518 observed glycomic changes[6]. Furthermore, the increased expression of oligomannose-type
519 *N*-glycan was accompanied by overall reduction of sialylated complex-type glycans on
520 cell-extracted and secreted proteins, irrespective of post-infection time points. We hypothesize
521 that the elevated expression of oligomannose-type *N*-glycans contributes to the downregulation
522 of sialylated complex-type *N*-glycans through two potential mechanisms. First, the
523 accumulation of oligomannose structures may saturate the glycosylation machinery within the
524 Golgi apparatus, thereby limiting the processing capacity for downstream glycan maturation.
525 Second, as the biosynthesis of complex-type *N*-glycans requires the prior trimming of
526 oligomannose precursors, excessive levels of these unprocessed glycans may reduce the
527 availability of appropriately processed substrates necessary for complex glycan formation[5].
528 Future studies incorporating transcriptomic and proteomic analysis will benefit from evaluating
529 the expression levels of Golgi-resident mannosidases and glycosyltransferases to confirm
530 whether elevated oligomannose levels contribute to the reduction in complex-type *N*-glycan
531 expression[6,42]. These studies, together with the existing glycomic data, may determine whether
532 the reduction in complex-type *N*-glycan expression upon HPIV-3 infection is caused by limited
533 substrate availability, as complex glycan synthesis requires the prior trimming of
534 oligomannose, or by saturation of the glycosylation machinery due to an overload of
535 oligomannose substrates.

536 Moreover, we were able to identify α2,3- and α2,6-linked isomers with the composition
537 of N4H5S1, based on chromatographic separation, together with MS fragmentation[43].
538 Interestingly, HPIV-3 infection leads to a lower expression of *N*-glycans containing α2,3-linked
539 sialic acid and an increase of its α2,6-linked counterpart, with the same composition (N4H5S1).
540 A previous study found that HPIV-3 utilizes α2,3- and α2,6-linked *N*-acetylneuraminic acid
541 (Neu5Ac) to galactose as receptors, with a higher HPIV-3 HN neuraminidase activity observed
542 for α2,3-linked Neu5Ac[20]. Thus, the downregulation of α2,3-linked sialylated isomeric

543 glycans, in this instance, could be attributed to the HPIV-3 HN neuraminidase activity,
544 mediating the cleavage of receptor glycans at the end of each viral replication cycle[44].
545 Furthermore, we hypothesize that higher expression of α2,6-linked isomer of N4H5S1 in
546 infected cells could be a consequence of the α2,3-linked sialic acid trimming of N4H5S2
547 (Figure S4, S6, S8, S10), as the HPIV-3 HN-mediated cleavage of N4H5S2 glycan would
548 potentially generate glycan with the composition of HN4H5N1. To confirm the intrinsic role
549 of HN protein on the reduction of sialylated *N*-glycans it would be interesting to treat infected
550 cells with a specific inhibitor to HN protein[45]. Moreover, as glycan biosynthesis is a sequential
551 enzymatic process, the modulation of sialylated complex-type *N*-glycans expression could also
552 be the result of virus infection-mediated changes in enzyme expression related to glycan
553 biosynthesis[27]. A bulk RNA-seq analysis of infected and mock-infected cells might enable us
554 to identify the expression profiles of enzymes involved in glycan biosynthesis, thereby
555 uncovering potential mechanisms underlying the observed changes in *N*-glycans upon
556 infection.

557 The impact of HPIV-3 infection in the host-cell *O*-glycome is significant and we have
558 observed that there is a significant reduction of core 2 type as well as a higher expression of
559 core 1 type *O*-glycans across host cell-extracted and secreted proteins. A recent study also
560 described an approximately 2.5-fold downregulation of core 2 *N*-acetylglucosamine transferase
561 (GlcNAcT) enzyme upon HPIV-3 infection on A549 cells[42]. We propose that the reduction of
562 core 2 type *O*-glycans could be the result of downregulation of the core 2
563 β1,6-*N*-acetylglucosaminyltransferase (Core 2 GlcNAc-T) enzyme that acts on core 1 type to
564 make core 2 type *O*-glycans. Furthermore, concomitant with the observed down regulation of
565 core 2 type *O*-glycans upon HPIV-3 infection, we also detected a down-regulation of doubly
566 sialylated core 2 type glycans with a corresponding higher expression of singly sialylated
567 core 2 type structures in infected cells. Similar for the downregulation of α2,3-linked sialylated
568 isomeric *N*-glycans, we infer that the reduction of doubly sialylated core 2 type structures is
569 caused by the neuraminidase activity of the HPIV-3 HN protein which subsequently results in
570 the upregulation of similar glycans with one less Neu5Ac[46]. Again, to verify the specific role
571 of the HPIV-3 HN protein in the reduction of doubly-sialylated *O*-glycans, it would be valuable
572 to treat infected cells with a specific inhibitor of the HN protein[45] and determine the expression
573 of doubly-sialylated *O*-glycans. Nonetheless, these changes may have profound implications
574 for host-cell glycosylation profiles, influencing immune responses and potentially contributing
575 to the pathogenesis of the virus[6,42].

576 GSL glycans significantly contribute to the formation of cellular glycome and some
577 viruses including HPIV-3 are known to exploit GSL glycans in their life cycle[20]. In our analysis,
578 gangliosides account for approximately 60% of the total GSL glycan population in A549 cells,
579 underscoring their dominance in the glycan landscape of the respiratory epithelium. HPIV-3
580 triggers altered expression of gangliosides glycans including GM1, GM3, and GD3, which are
581 often implicated in viral replication cycle[24]. These gangliosides have been previously
582 implicated in modulating viral replication, either by serving as entry cofactors or by influencing
583 intracellular signalling pathways essential for viral propagation[47,48]. For example, GM1 serves
584 as entry receptors for simian virus 40 (SV40)[49], while GM3 plays a dual role in cell
585 physiology[50] and viral pathogenesis, including facilitating influenza virus infection by
586 modulating membrane dynamics and virus-host interactions[51]. Furthermore, GM3 has been
587 shown to regulate cell proliferation and differentiation by modulating receptor tyrosine kinases
588 such as epidermal growth factor receptor (EGFR)[52]. During viral infection, these signalling
589 pathways are often hijacked to support viral replication and suppress host antiviral
590 responses[53,54]. GD3 ganglioside is also implicated in viral infection, particularly those affecting
591 nervous system[55]. Altogether, changes in ganglioside expression during HPIV-3 infection
592 might represent either a viral adaptation to enhance conditions for its replication, or a host-cell
593 mechanism to manage the infection.

594 The second most common type of GSL glycans detected in A549 cells was the
595 neo(lacto)-series. A previous study reported a sialylated neo(lacto)-series glycan as a potential
596 receptor for HPIV-3[20,46]. In our study we found a potential sialylated neo(lacto)-series glycan
597 was downregulated upon HPIV-3 infection. We hypothesize that the cleavage of sialic acid,
598 mediated by HPIV-3 HN, may contribute to the reduction of sialylated neo(lacto)-series
599 glycans on HPIV-3 infected cells. Furthermore, few other glycans, which were not recognised
600 as binding factors, have also been found to be altered after HPIV-3 infection in our study. We
601 hypothesize a similar receptor specificity analysis using altered GSL glycans (GM1, GM3,
602 GD3) could potentially identify few other GSL glycans as binding factors.

603 Conclusion

604 Using advanced mass spectrometry-based glycomics, we investigated HPIV-3–induced
605 alterations in the glycome of A549 human lung epithelial cells. Our analysis revealed
606 approximately 116 distinct glycan species in both HPIV-3–infected and mock-infected cells,
607 highlighting the complexity and diversity of the host-cell glycome. Importantly, this study

provides the first experimental evidence that HPIV-3 infection induces marked alterations in the host cell glycome, spanning all three major glycan types (*N*-, *O*-, and glycosphingolipid glycans). These alterations suggest that HPIV-3 infection significantly remodels the host cell surface and secretory glycan landscape, potentially influencing key biological processes such as virus-host interactions, immune recognition, and intracellular signalling. Furthermore, our analytical approach provides a valuable platform for characterizing virus-induced glycomic changes and can be readily adapted to study other respiratory viruses, e.g., influenza virus, thereby paving the way for a better understanding of the roles of glycans in viral pathogenesis.

Acknowledgement

This research was partially funded by Griffith University International Postgraduate Research Scholarship (GUIPRS) and Griffith University Postgraduate Research Scholarship (GUPRS) (P.K.D). We gratefully acknowledge funding from the National Health and Medical Research Council (NHMRC) (MvI., APP1047824 & GNT1196520) and a Peter Doherty Biomedical Early Career Fellowship (L.D., GNT1157150). We thank Dr. Thomas Litfin and Anuk Indraratna for assisting in data visualization.

Author contributions

Conceptualisation: P.K.D., L.D., B.B., P.G., A.E.D, M.v.I.; methodology: P.K.D., P.G., A.E.D.; investigation: P.K.D.; analysis: P.K.D.; writing—original draft: P.K.D.; writing—review and editing: L.D., P.G., B.B., A.E.D., M.v.I.; funding acquisition: L.D., M.v.I.

Abbreviations,

HPIV: Human parainfluenza virus

HN: haemagglutinin-neuraminidase

H.p.i: Hour's post-infection

CEP: Cell extracted protein

SP: Secreted protein

HN: *N*-acetylglucosamine

H: Hexose

dH: Deoxyhexose

Man: Mannose

N: *N*-acetylneuraminic Acid

638 G: *N*-glycolylneuraminic Acid
639 GSL: Glycosphingolipids
640 PGC: Porous graphitized carbon
641 ESI: Electrospray ionization
642 CID: Collision induced dissociation.
643

Reference

644 1. Branche, A. R. & Falsey, A. R. Parainfluenza Virus Infection. *Semin. Respir. Crit.*
645 *Care Med.* **37**, 538–554 (2016).

646 2. Castleman, W. L., Northrop, P. J. & McAllister, P. K. Replication of parainfluenza
647 type-3 virus and bovine respiratory syncytial virus in isolated bovine type-II
648 alveolar epithelial cells. *Am. J. Vet. Res.* **52**, 880–885 (1991).

649 3. Castleman, W. L., Northrop, P. J. & McAllister, P. K. Replication of parainfluenza
650 type-3 virus and bovine respiratory syncytial virus in isolated bovine type-II
651 alveolar epithelial cells. *Am. J. Vet. Res.* **52**, 880–885 (1991).

652 4. Saha, S., Grimwood, K., Lambert, S. B., Sarna, M. & Ware, R. S. Parainfluenza
653 Virus Infection in an Australian Community-based Birth Cohort. *Pediatr. Infect.*
654 *Dis. J.* **39**, e284 (2020).

655 5. Reily, C., Stewart, T. J., Renfrow, M. B. & Novak, J. Glycosylation in health and
656 disease. *Nat. Rev. Nephrol.* **15**, 346–366 (2019).

657 6. Heindel, D. W. *et al.* Glycomic analysis of host response reveals high mannose as
658 a key mediator of influenza severity. *Proc. Natl. Acad. Sci. U. S. A.* **117**, 26926–
659 26935 (2020).

660 7. Quiñones-Kochs, M. I., Buonocore, L. & Rose, J. K. Role of N-Linked Glycans
661 in a Human Immunodeficiency Virus Envelope Glycoprotein: Effects on Protein
662 Function and the Neutralizing Antibody Response. *J. Virol.* **76**, 4199–4211 (2002).

663 8. Watanabe, Y., Bowden, T. A., Wilson, I. A. & Crispin, M. Exploitation of
664 glycosylation in enveloped virus pathobiology. *Biochim. Biophys. Acta Gen. Subj.*
665 **1863**, 1480–1497 (2019).

666 9. Dirr, L. *et al.* The catalytic mechanism of human parainfluenza virus type 3
667 haemagglutinin-neuraminidase revealed. *Angew. Chem. Int. Ed Engl.* **54**, 2936–
668 2940 (2015).

669 10. Donohoo, K. B. *et al.* Advances in mass spectrometry-based glycomics-An update
670 covering the period 2017-2021. *Electrophoresis* **43**, 119–142 (2022).

671 11. Zhang, T. *et al.* Differential O- and Glycosphingolipid Glycosylation in Human
672 Pancreatic Adenocarcinoma Cells With Opposite Morphology and Metastatic
673 Behavior. *Front. Oncol.* **10**, 732 (2020).

674 12. Jensen, P. H., Karlsson, N. G., Kolarich, D. & Packer, N. H. Structural analysis of
675 N- and O-glycans released from glycoproteins. *Nat. Protoc.* **7**, 1299–1310 (2012).

676 13. Wang, D. *et al.* Glycosphingolipid-Glycan Signatures of Acute Myeloid Leukemia
677 Cell Lines Reflect Hematopoietic Differentiation. *J. Proteome Res.* **21**, 1029–
678 1040 (2022).

679 14. MacLean, B. *et al.* Skyline: an open source document editor for creating and
680 analyzing targeted proteomics experiments. *Bioinformatics* **26**, 966–968 (2010).

681 15. Cooper, C. A., Gasteiger, E. & Packer, N. H. GlycoMod--a software tool for
682 determining glycosylation compositions from mass spectrometric data.
683 *Proteomics* **1**, 340–349 (2001).

684 16. Ceroni, A. *et al.* GlycoWorkbench: A Tool for the Computer-Assisted Annotation
685 of Mass Spectra of Glycans. *J. Proteome Res.* **7**, 1650–1659 (2008).

686 17. Campbell, M. P. & Packer, N. H. UniCarbKB: New database features for
687 integrating glycan structure abundance, compositional glycoproteomics data, and
688 disease associations. *Biochim. Biophys. Acta* **1860**, 1669–1675 (2016).

689 18. Everest-Dass, A. V., Abrahams, J. L., Kolarich, D., Packer, N. H. & Campbell, M.
690 P. Structural Feature Ions for Distinguishing ***N-*** and ***O-*** Linked Glycan Isomers
691 by LC-ESI-IT MS/MS. *J. Am. Soc. Mass Spectrom.* **24**, 895–906 (2013).

692 19. Crouch, L. I. *et al.* The role of glycans in health and disease: Regulators of the
693 interaction between gut microbiota and host immune system. *Semin. Immunol.* **73**,
694 101891 (2024).

695 20. Suzuki, T. *et al.* Receptor specificities of human respiroviruses. *J. Virol.* **75**, 4604–
696 4613 (2001).

697 21. Abrahams, J. L., Campbell, M. P. & Packer, N. H. Building a PGC-LC-MS N-
698 glycan retention library and elution mapping resource. *Glycoconj. J.* **35**, 15–29
699 (2018).

700 22. Anugraham, M. *et al.* Specific glycosylation of membrane proteins in epithelial
701 ovarian cancer cell lines: glycan structures reflect gene expression and DNA
702 methylation status. *Mol. Cell. Proteomics MCP* **13**, 2213–2232 (2014).

703 23. Olofsson, S., Bally, M., Trybala, E. & Bergström, T. Structure and Role of O-
704 Linked Glycans in Viral Envelope Proteins. *Annu. Rev. Virol.* **10**, 283–304 (2023).

705 24. Aerts, J. M. F. G., Artola, M., van Eijk, M., Ferraz, M. J. & Boot, R. G.
706 Glycosphingolipids and Infection. Potential New Therapeutic Avenues. *Front.*
707 *Cell Dev. Biol.* **7**, 324 (2019).

708 25. Lingwood, C. A. & Branch, D. R. The role of glycosphingolipids in HIV/AIDS.
709 *Discov. Med.* **11**, 303–313 (2011).

710 26. Taube, S., Jiang, M. & Wobus, C. E. Glycosphingolipids as Receptors for Non-
711 Enveloped Viruses. *Viruses* **2**, 1011–1049 (2010).

712 27. Schjoldager, K. T., Narimatsu, Y., Joshi, H. J. & Clausen, H. Global view of human
713 protein glycosylation pathways and functions. *Nat. Rev. Mol. Cell Biol.* **21**, 729–
714 749 (2020).

715 28. Bagdonaite, I. & Wandall, H. H. Global aspects of viral glycosylation.
716 *Glycobiology* **28**, 443–467 (2018).

717 29. Hargett, A. A. & Renfrow, M. B. Glycosylation of viral surface proteins probed
718 by mass spectrometry. *Curr. Opin. Virol.* **36**, 56–66 (2019).

719 30. Feng, T. *et al.* Glycosylation of viral proteins: Implication in virus–host interaction
720 and virulence. *Virulence* **13**, 670–683 (2022).

721 31. Markine-Goriaynoff, N. *et al.* Glycosyltransferases encoded by viruses. *J. Gen.*
722 *Virol.* **85**, 2741–2754 (2004).

723 32. Singh, S. *et al.* Loss of α-gal during primate evolution enhanced antibody-effector
724 function and resistance to bacterial sepsis. *Cell Host Microbe* **29**, 347-361.e12
725 (2021).

726 33. Altman, M. O. & Gagneux, P. Absence of Neu5Gc and Presence of Anti-Neu5Gc
727 Antibodies in Humans—An Evolutionary Perspective. *Front. Immunol.* **10**, 789
728 (2019).

729 34. Larsen, M. D. *et al.* Afucosylated IgG characterizes enveloped viral responses and
730 correlates with COVID-19 severity. *Science* **371**, eabc8378 (2021).

731 35. Chakraborty, S. *et al.* Proinflammatory IgG Fc structures in patients with severe
732 COVID-19. *Nat. Immunol.* **22**, 67–73 (2021).

733 36. Read, A. & Schröder, M. The Unfolded Protein Response: An Overview. *Biology*
734 **10**, 384 (2021).

735 37. Wong, M. Y. *et al.* XBP1s activation can globally remodel N-glycan structure
736 distribution patterns. *Proc. Natl. Acad. Sci.* **115**, E10089–E10098 (2018).

737 38. Victor, P., Sarada, D. & Ramkumar, K. M. Crosstalk between endoplasmic
738 reticulum stress and oxidative stress: Focus on protein disulfide isomerase and
739 endoplasmic reticulum oxidase 1. *Eur. J. Pharmacol.* **892**, 173749 (2021).

740 39. Carreras-Sureda, A., Pihán, P. & Hetz, C. Calcium signaling at the endoplasmic
741 reticulum: fine-tuning stress responses. *Cell Calcium* **70**, 24–31 (2018).

742 40. Slaine, P. D. *et al.* Thiopurines Activate an Antiviral Unfolded Protein Response
743 That Blocks Influenza A Virus Glycoprotein Accumulation. *J. Virol.* **95**,
744 10.1128/jvi.00453-21 (2021).

745 41. Rufo, N., Garg, A. D. & Agostinis, P. The Unfolded Protein Response in
746 Immunogenic Cell Death and Cancer Immunotherapy. *Trends Cancer* **3**, 643–658
747 (2017).

748 42. Blanco-Melo, D. *et al.* Imbalanced Host Response to SARS-CoV-2 Drives
749 Development of COVID-19. *Cell* **181**, 1036-1045.e9 (2020).

750 43. Anugraham, M. *et al.* Specific Glycosylation of Membrane Proteins in Epithelial
751 Ovarian Cancer Cell Lines: Glycan Structures Reflect Gene Expression and DNA
752 Methylation Status. *Mol. Cell. Proteomics MCP* **13**, 2213–2232 (2014).

753 44. Amonsen, M., Smith, D. F., Cummings, R. D. & Air, G. M. Human Parainfluenza
754 Viruses hPIV1 and hPIV3 Bind Oligosaccharides with α2-3-Linked Sialic Acids
755 That Are Distinct from Those Bound by H5 Avian Influenza Virus Hemagglutinin.
756 *J. Virol.* **81**, 8341–8345 (2007).

757 45. Guillon, P. *et al.* Structure-guided discovery of potent and dual-acting human
758 parainfluenza virus haemagglutinin-neuraminidase inhibitors. *Nat. Commun.* **5**,
759 5268 (2014).

760 46. Amonsen, M., Smith, D. F., Cummings, R. D. & Air, G. M. Human Parainfluenza
761 Viruses hPIV1 and hPIV3 Bind Oligosaccharides with α2-3-Linked Sialic Acids
762 That Are Distinct from Those Bound by H5 Avian Influenza Virus Hemagglutinin.
763 *J. Virol.* **81**, 8341 (2007).

764 47. Das, A. *et al.* Gangliosides are essential endosomal receptors for quasi-enveloped
765 and naked hepatitis A virus. *Nat. Microbiol.* **5**, 1069–1078 (2020).

766 48. Mazzon, M. & Mercer, J. Lipid interactions during virus entry and infection. *Cell.*
767 *Microbiol.* **16**, 1493–1502 (2014).

768 49. Tsai, B. *et al.* Gangliosides are receptors for murine polyoma virus and SV40.
769 *EMBO J.* **22**, 4346–4355 (2003).

770 50. Nojiri, H., Takaku, F., Terui, Y., Miura, Y. & Saito, M. Ganglioside GM3: an acidic
771 membrane component that increases during macrophage-like cell differentiation
772 can induce monocytic differentiation of human myeloid and monocytoid leukemic
773 cell lines HL-60 and U937. *Proc. Natl. Acad. Sci.* **83**, 782–786 (1986).

774 51. Vrijens, P. *et al.* Influenza virus entry via the GM3 ganglioside-mediated platelet-
775 derived growth factor receptor β signalling pathway. *J. Gen. Virol.* **100**, 583–601
776 (2019).

777 52. Coskun, Ü., Grzybek, M., Drechsel, D. & Simons, K. Regulation of human EGF
778 receptor by lipids. *Proc. Natl. Acad. Sci. U. S. A.* **108**, 9044–9048 (2011).

779 53. Ryu, J.-S. *et al.* Ganglioside GM3 Up-Regulate Chondrogenic Differentiation by
780 Transform Growth Factor Receptors. *Int. J. Mol. Sci.* **21**, 1967 (2020).

781 54. Fan, Y., Sanyal, S. & Bruzzone, R. Breaking Bad: How Viruses Subvert the Cell
782 Cycle. *Front. Cell. Infect. Microbiol.* **8**, 396 (2018).

783 55. Cutillo, G., Saariaho, A.-H. & Meri, S. Physiology of gangliosides and the role of
784 antiganglioside antibodies in human diseases. *Cell. Mol. Immunol.* **17**, 313–322
785 (2020).

Supplementary Figures

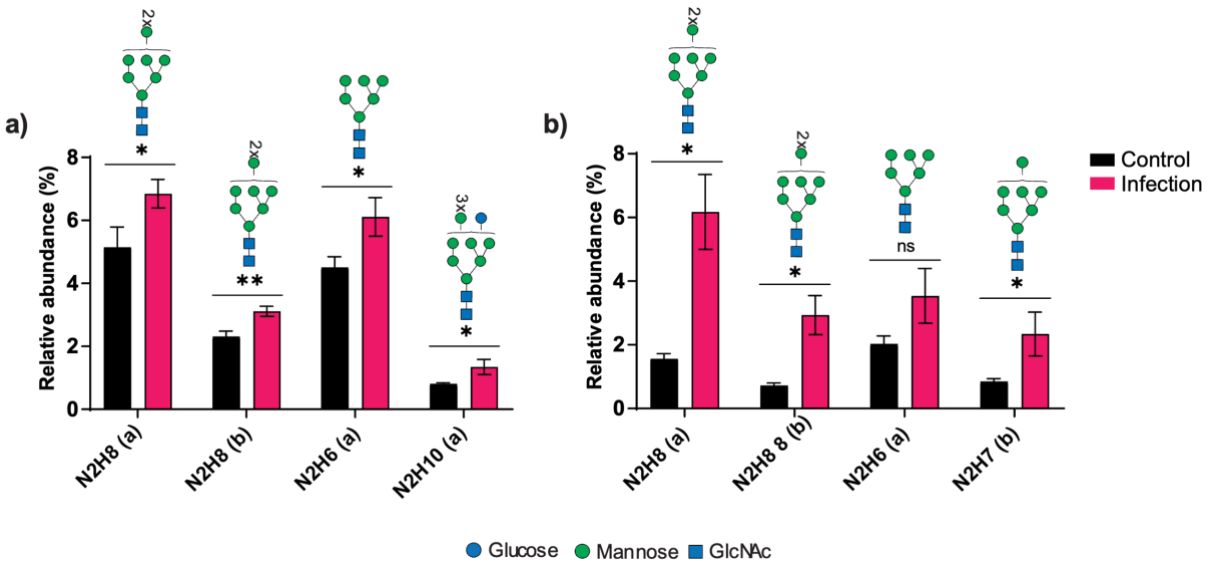

Fig S1. ***Alterations of oligomannose-type* N*-glycan on mock-infected and infected cells at 24 h post-infection.*** *Relative abundance of significantly altered oligomannose type glycans on a) cell extracted proteins, b) secreted proteins. Man: Mannose; Glc: Glucose. n=3, *P<0.05, **P<0.01, ns: not significant, unpaired Welch's t-test.*

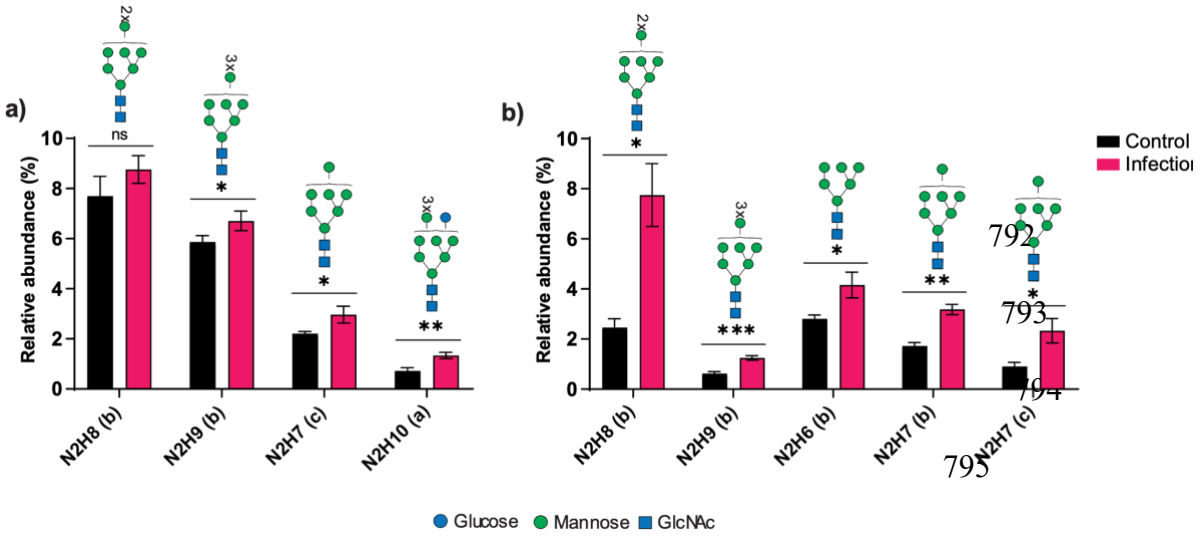

Fig S2: ***Alteration of oligomannose type* N*-glycan on mock-infected and infected cells at 48 h post-infection.*** *Relative abundance of significantly altered oligomannose type glycans on a) cell extracted proteins, b) secreted proteins. Man: Mannose; Glc: Glucose. n=3, *P<0.05, **P<0.01, ns: not significant, unpaired Welch's t-test.*

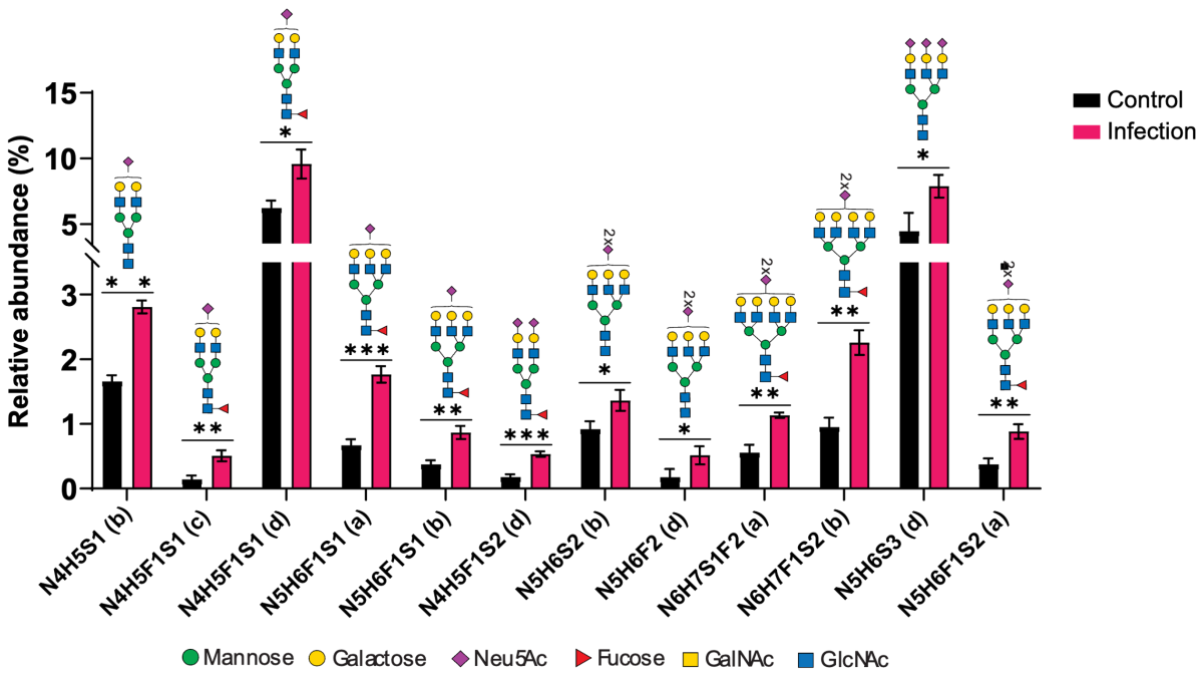

Fig S3: Significantly altered (increased expression) sialylated complex-type N-*glycan species on cell extracted proteins at 24h post-infection. n=3, *P<0.05, **P<0.01, ***P<0.001, unpaired Welch's t-test. N:* N-*acetylhexosamine; H: Hexose; F: Fucose; S:* N-*acetylneuraminic Acid.*

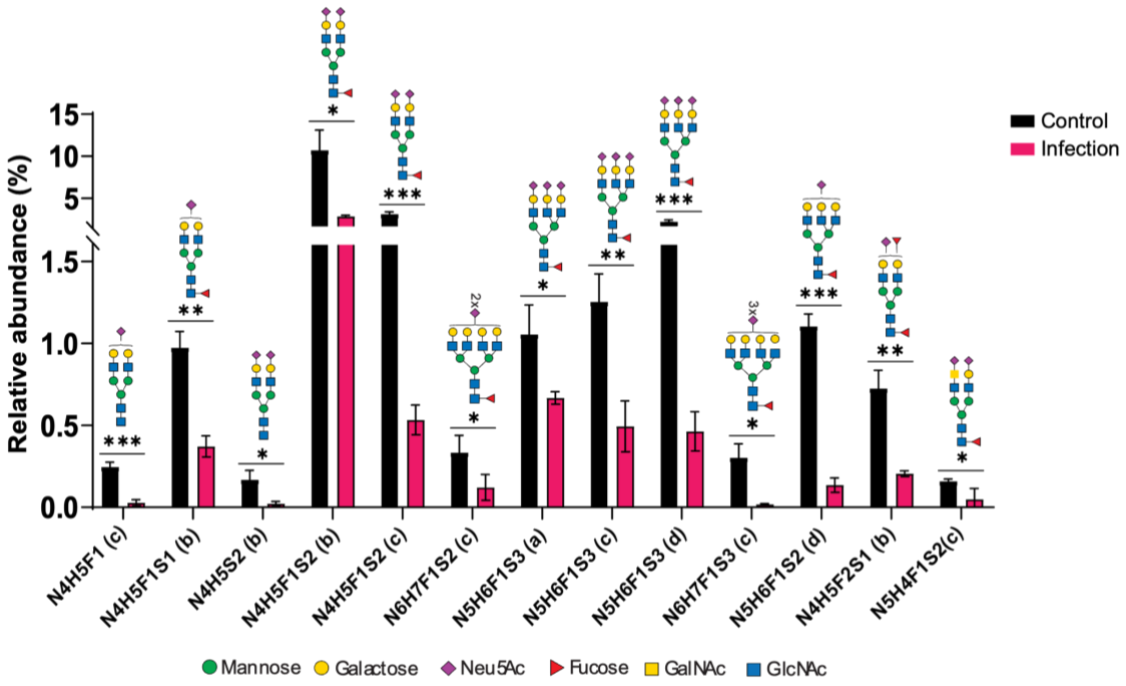

*Fig S4: Significantly altered (decreased expression) sialylated complex-type N-glycan species on cell extracted proteins at 24h post-infection. n=3, *P<0.05, **P<0.01, ***P<0.001, unpaired Welch's t-test. N:* N-*acetylhexosamine; H: Hexose; F: Fucose; S:* N-*acetylneuraminic Acid.*

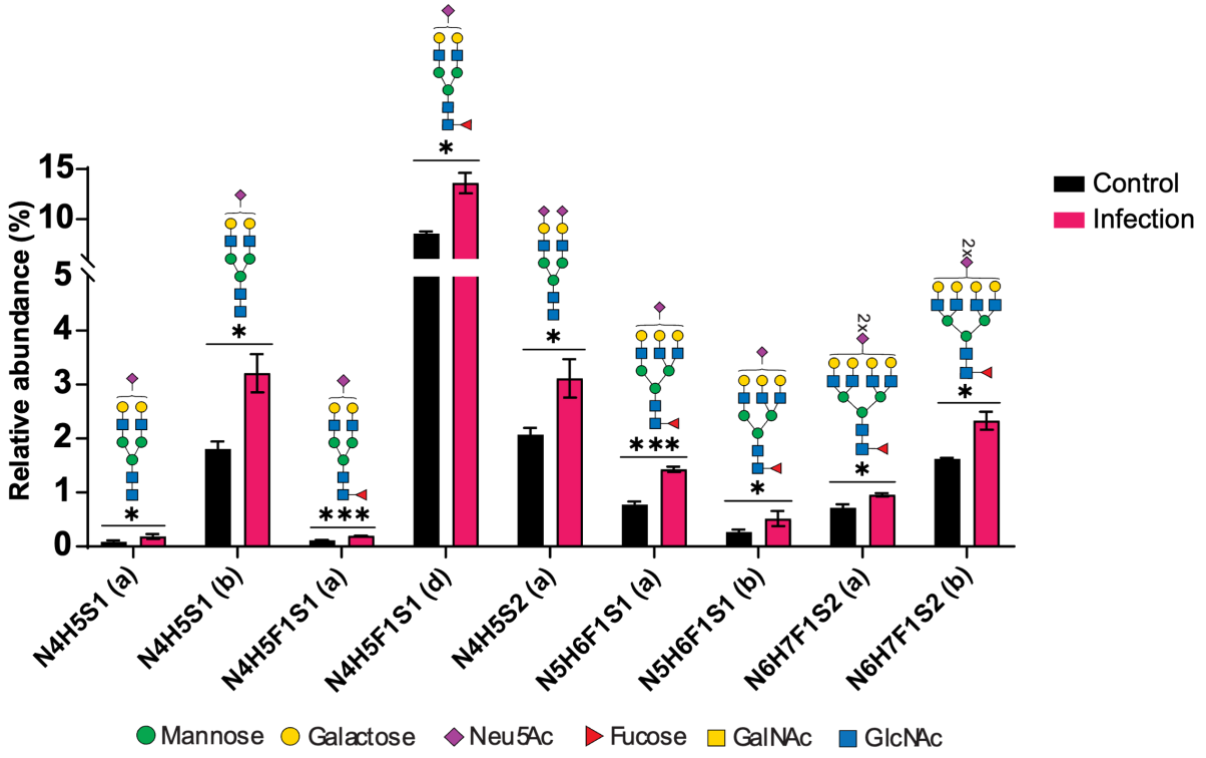

Fig S5: Significantly altered (increased expression) sialylated complex-type N-*glycan species on secreted proteins at 24h post-infection. n=3, *P<0.05, **P<0.01, ***P<0.001, unpaired Welch's t-test. N:* N-*acetylhexosamine; H: Hexose; F: Fucose; S:* N-*acetylneuraminic Acid.*

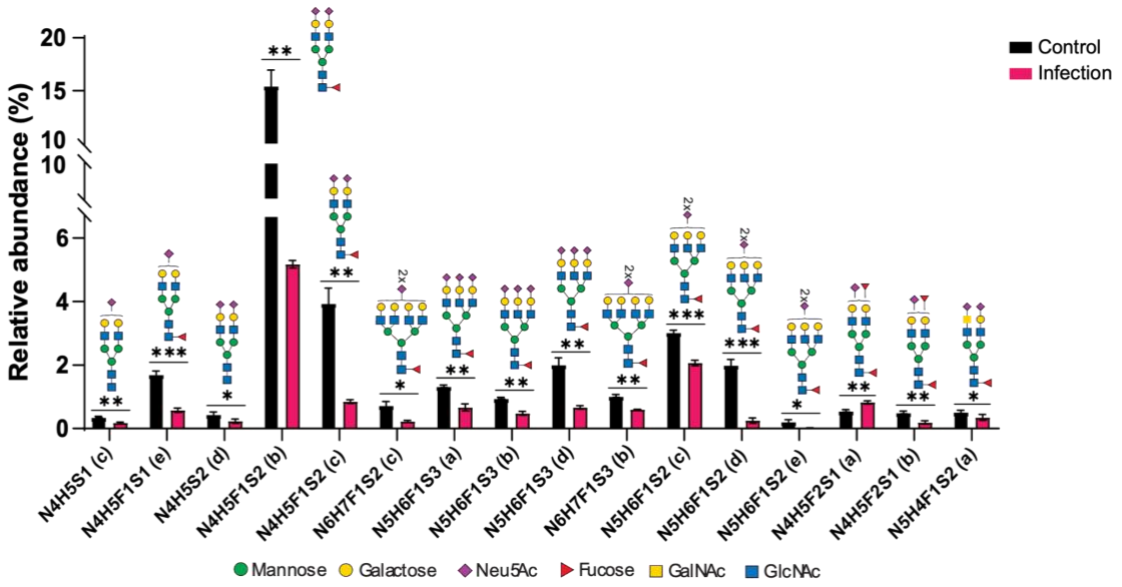

Fig S6: Significantly altered (decreased expression) sialylated complex-type N-*glycan species on secreted proteins at 24h post-infection. n=3, *P<0.05, **P<0.01, ***P<0.001, unpaired Welch's t-test. N:* N-*acetylhexosamine; H: Hexose; F: Fucose; S:* N-*acetylneuraminic Acid.*

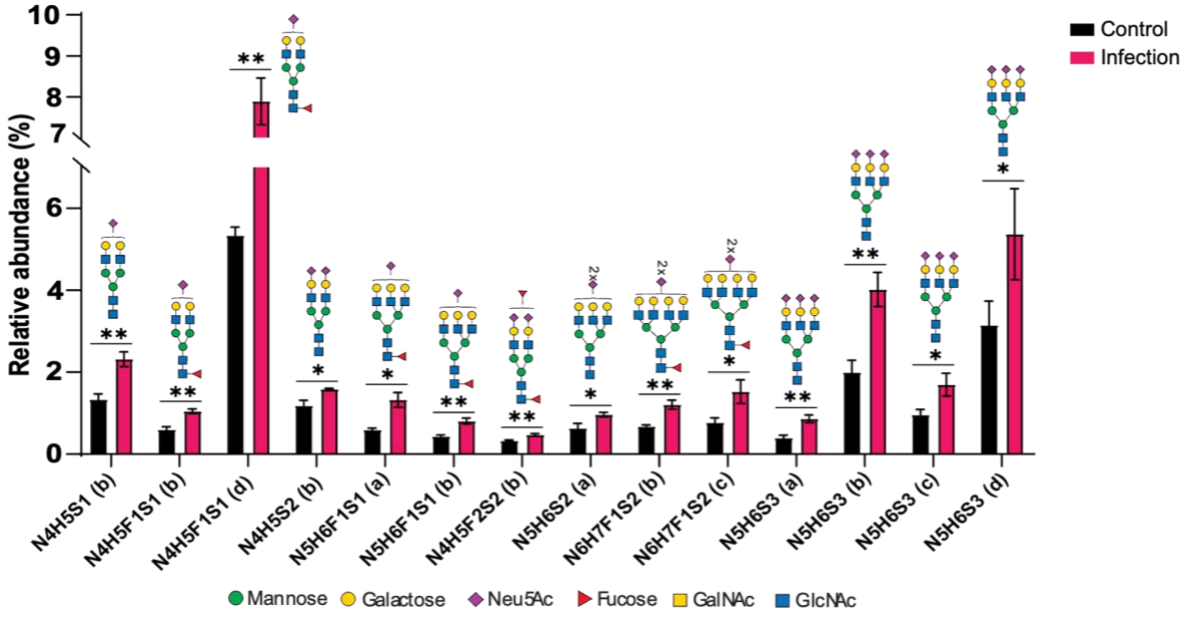

Fig S7: Significantly altered (increased expression) sialylated complex-type N-*glycan species on cell extracted proteins at 48h post- infection. n=3, *P<0.05, **P<0.01, ***P<0.001, unpaired Welch's t-test. N:* N-*Acetyl Hexosamine; H: Hexose; F: Fucose; S:* N-*acetylheuraminic Acid.*

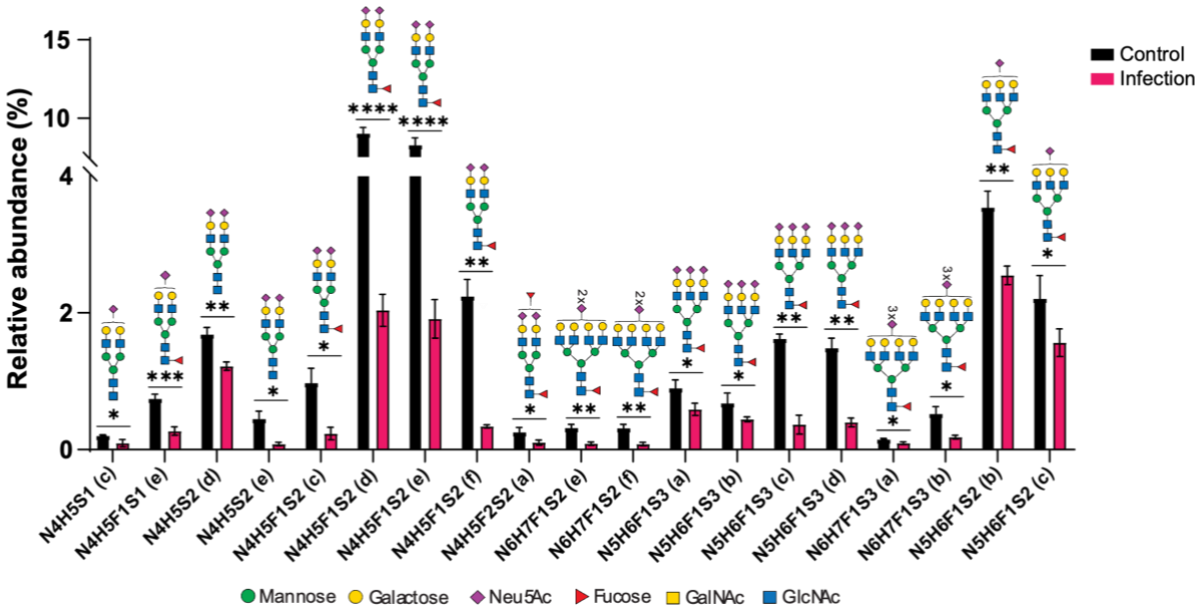

Fig S8: Significantly altered (decreased expression) sialylated complex-type N-*glycan species on cell extracted proteins at 48h post- infection. n=3, *P<0.05, **P<0.01, ***P<0.001, ****P<0.0001, unpaired Welch's t-test. N:* N-*acetylhexosamine; H: Hexose; F: Fucose; S:* N-*acetylneuraminic Acid.*

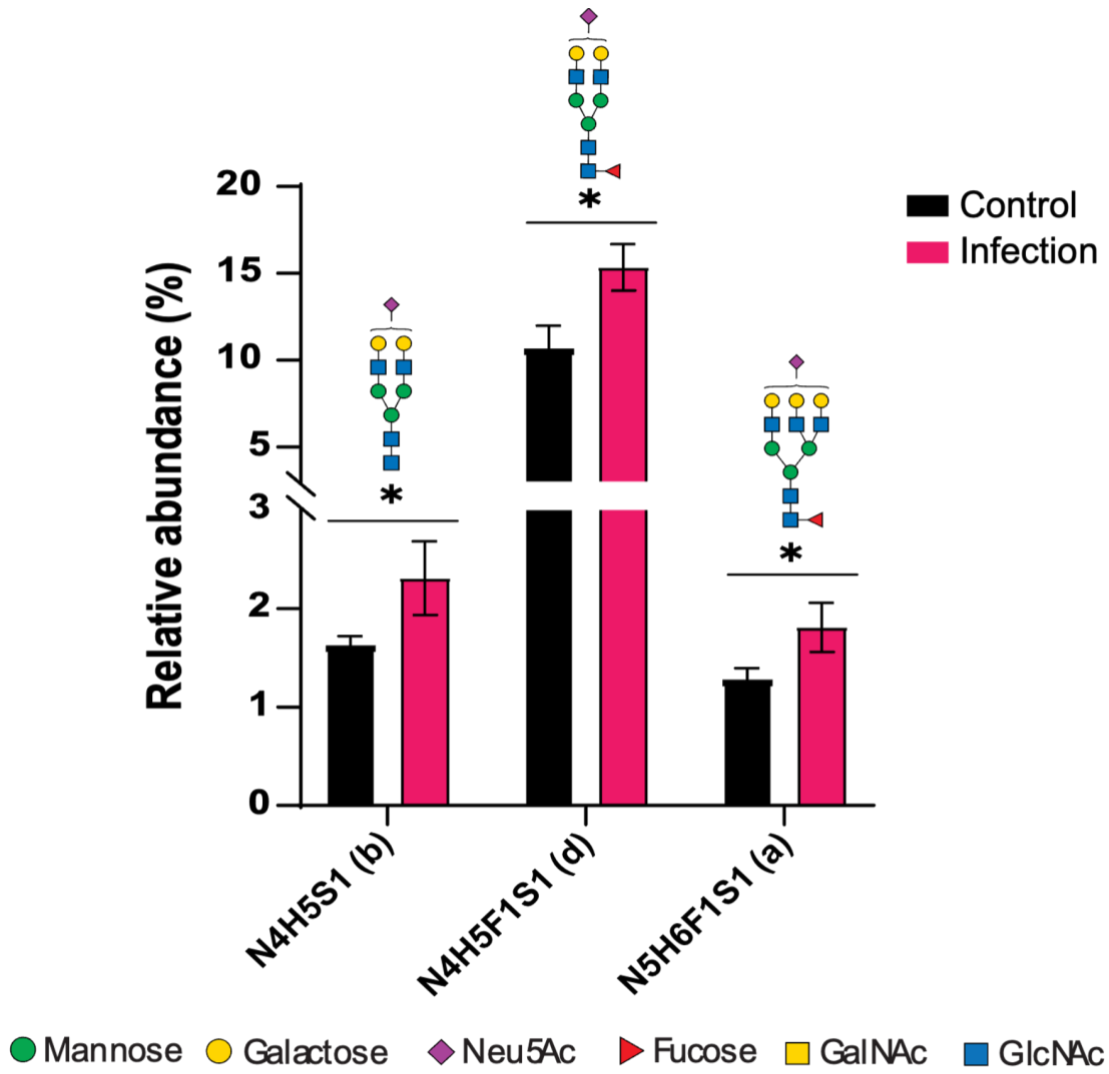

833

834 *Fig S9: Significantly altered (increased expression) sialylated complex-type* N-*glycan species on secreted proteins at 48h*
835 *post-infection. n=3, *P<0.05, **P<0.01, unpaired Welch's t-test. N: N-acetylhexosamine; H: Hexose; F: Fucose;*
836 *S:* N-*acetylneuraminic Acid.*

837

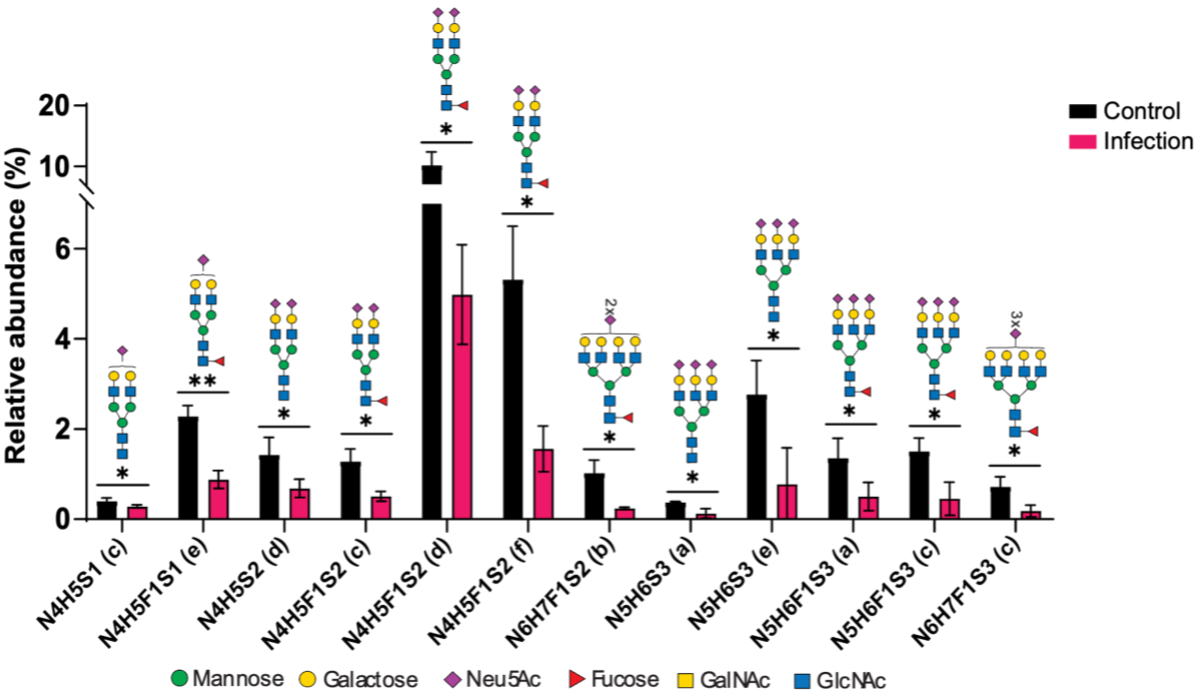

838

839 *Fig S10: Significantly altered (decreased expression) sialylated complex-type* N-*glycan species on secreted proteins at 48h*
840 *post-infection. n=3, *P<0.05, **P<0.01, unpaired Welch's t-test. N:* N-*acetylhexosamine; H: Hexose; F: Fucose;*
841 *S:* N-*acetylneuraminic Acid.*